

EUROPEAN ORGANIZATION FOR NUCLEAR RESEARCH

INTERSECTING STORAGE RINGS COMMITTEE

MEASUREMENT OF THE ELASTIC SCATTERING CROSS-SECTION

AT THE ISR

P. Darriulat, C. Rubbia, P. Strolin and K. Tittel

CERN

G. Diambrini, I. Giannini, P. Ottonello, A. Santroni, G. Sette

INFN - Sezione di Genova

V. Bisi, A. Germak, C. Grosso, M.I. Ferrero

INFN - Sezione di Torino

A B S T R A C T

An experiment intended to observe the elastic proton-proton events at the ISR is discussed. The whole angular range from 1 mrad to about 100 mrad can be covered. The very small angle events are detected by a two-arm spectrometer sharing with the storage ring system the first four magnets. The larger angle events are momentum analyzed with a pair of magnets which do not perturb the circulating beam. Extensive use of elastic scattering on residual hydrogen gas is made in order to calibrate the spectrometers and to determine the angular and space distribution of circulating beams at the interaction point.

(Proposal)

CERN LIBRARIES, GENEVA



CM-P00063149

Geneva - 15 March, 1969.

1. INTRODUCTION

1.1 Historical preface

The determination of the differential elastic p-p cross-section up to the highest available energies is probably one of the most evident parts of the experimental program around the ISR. A great deal of study work has been performed on this topic, since the early days of the ISR design. Experimental arrangements for studying p-p elastic scattering have been discussed at that time by Jones and de Raad¹⁾ (1962), de Raad²⁾ (1962), Jones³⁾ (1963) and Terwilliger⁴⁾ (1963).

Accurate angle measurements on both outgoing protons make possible an efficient rejection of inelastic events. Jones³⁾ has estimated that for the inelastic event:

$$p + p \rightarrow p + N^* \rightarrow p + p + \pi^0$$

where N^* has the mass of 1.5 GeV, the fraction of the N^* events which could be confused with elastic scattering is less than 10^{-3} [see also Minten⁵⁾ (1968)].

Momentum analysis of both outgoing particles is possible [de Raad²⁾ (1963)] replacing the magnet units adjacent to the region of interaction by bending magnets with uniform field and by quadrupole lenses. For a larger acceptance Jones³⁾ has proposed the use of an air core magnetic field arranged in a way such as not to perturb the circulating beam.

More recently (1968), a working group⁶⁾ (G. Cocconi, L. di Lella and three of us -- P.D., C.R. and P.S.) has reconsidered the very small angle elastic scattering, following a proposal by G. Cocconi⁷⁾ to determine the ISR luminosity from the known Coulomb differential cross-section. The experiment appears feasible, observing both diffused particles at about $\frac{1}{4}$ betatron wavelength downstream from the interaction point. Protons could be detected either by a counter matrix introduced inside the vacuum chamber [Jones³⁾ (1963)] or by a pair of septum magnets and secondary magnetic channels [P. Darriulat and P. Strolin⁶⁾ (1968)]. Monte Carlo calculations [P. Darriulat and L. di Lella⁶⁾ (1968)] have shown that the distortion of the angular distribution due to the finite momentum and angular spreads can easily be accounted for, down to the smallest angles ($\theta < 1$ mR). These conclusions have been strengthened by more recent

calculations by U. Amaldi, G. Matthiae and P. Strolin⁸⁾ (1969).

An alternative approach to the very small-angle elastic scattering has been discussed by P. Darriulat and C. Rubbia⁹⁾. The authors have remarked that the "apparent" scattering angle could be considerably magnified adding quadrupole lenses in the interaction region (high $-\beta$ insertions).

The determination of the absolute elastic cross-section requires a measurement of the luminosity of the machine. In addition to the normalization on the Coulomb scattering [Cocconi⁷⁾ (1968)], several different methods for determining the luminosity have been proposed [Darriulat and Rubbia¹⁰⁾, Van der Meer¹¹⁾ and A.P. Onuchin and Steinberger¹²⁾]. It is believed that by one or more of these methods it will be possible to determine the machine luminosity to a high degree of accuracy ($< 1 \div 2\%$).

1.2 Experimental program

The main pieces of experimental information which could hopefully be extracted from the presently proposed experiment, are relative to three different angle regions: the very small angles (Coulomb-nuclear interference); the "diffraction" region and the large-angle region. The smallest scattering angle which can be observed is limited to about 1 mr, mainly because of the size and angular divergence of the circulating beams. The largest scattering angle is determined by counting rates. Assuming the nominal ISR luminosity:

$$L_{\max} = 4 \times 10^{-30} \text{ cm}^{-2} \text{ sec}^{-1},$$

it is expected that the elastic differential cross-section $d\sigma/dt$ will be explored over about ten orders of magnitude below the forward scattering cross-section. According to extrapolations¹³⁾ based on experiments at present energies, it is predicted that this largest scattering angle should occur somewhere between 50 mr and 100 mr (at 25 + 25 GeV/c). The experiment has consequently been designed in order to detect scattered protons from about 1 mr up to 120 mr.

We have divided the angle range into two main overlapping regions. The first one, from about 1 mr up to 6 mr can be covered extracting both scattered protons from the ISR vacuum chamber at 27 metres from the interaction point with septum magnets⁶⁾.

The arrangement consists of a pair of magnetic spectrometers, one for each scattered proton, sharing with the circulating beams the first four gradient magnets of the inner arc. The detecting counters are located at the focus of the spectrometers, well shielded and far away from the ISR beams. The second arrangement, designed to cover the angle range from 3.5 mR to 120 mR, detects scattered particles which escape from the ISR chamber within the some 9.5 free metres of the interaction region. For larger angles (> 10 mR) where the elastically scattered protons are expected to be considerably fewer than the particles produced in beam-beam and beam-gas interactions, magnetic analysis is foreseen. Spectrometer magnets do not perturb the circulating beam.

The two arrangements use the same monitoring and luminosity measuring systems.

An important feature of the experiment is based on the remark that the forward-emitted proton elastically scattered on residual hydrogen gas, is kinematically almost identical to the beam-beam elastic scatters. The beam-gas events can be detected observing the recoil proton emitted around 90° which acts as some sort of "lever arm" for the forward one.

Several types of beam observing devices are proposed in order to determine the beam profiles and their spatial and angular shapes. The determination of these parameters is very essential in the very small angle measurements.

2. THE SMALL ANGLE DETECTOR

2.1 Real part of the scattering amplitude

The main experimental problems to be investigated are briefly discussed. In the region of Coulomb-nuclear interference, assuming spin-independence, we can write the differential cross-section as:

$$\frac{d\sigma}{dt} = |A_c(1 + 2i\eta) + iA_{NI}(1 - i\alpha)|^2$$

where $t = -2p^2(1 - \cos \theta) \approx p^2\theta^2$ is the square of the four-momentum transfer in $(\text{GeV}/c)^2$, A_c is the real part of the Coulomb scattering amplitude. The imaginary contribution is $\eta = 1/137 \ln(1.06/ka\theta)$, where a is the radial parameter for the p-p interactions. With $a = 0.97$ fm,

$2\eta \sim 0.023$ at $t = -2 \times 10^{-3} \text{ (GeV/c)}^2$. For larger momentum transfers this contribution is even smaller. For small t values:

$$A_c = \frac{2 e^2}{c\beta|t|} (1 + 8t)$$

where the term $8t$ includes the effect of the electromagnetic form factor taken from e - p scattering. A_{NI} is the imaginary part of the nuclear scattering amplitude and α is the ratio of the real and imaginary parts of the amplitude. A_{NI} at $t = 0$ is given by the optical theorem and the t -dependence is to be taken from scattering at larger t values:

$$A_{\text{NI}} = \left(\frac{\sigma_{\text{T}}}{4\sqrt{\pi} \hbar} \right) e^{-at/2} .$$

At PS energies $a = \text{const} = \sim 10 \text{ (GeV/c)}^{-2}$. The experimental results are shown in Fig. 1 for the laboratory energy interval $8 \div 26 \text{ GeV/c}$, together with the predictions of dispersion relations of Söding¹⁴⁾.

The value of α decreases with increasing momentum (Fig. 1). Two different theoretical models based on Regge poles^{15,16)} predict a sizeable real part, at least in the lower part of the energy interval of the ISR, where also observation would be easiest because of the large scattering angles. Both models are adjusted to fit data on total cross-sections and real parts in the present energy range. The model of Cabibbo et al¹⁵⁾ assumes no Pomernanchuk trajectory [i.e. no trajectory with $\alpha_p(0) = 1$]. The other one¹⁶⁾ instead takes it into account and predicts a faster nuclear drop of the real part with increasing energy. Already at ISR energies of $2 \times 10 \text{ GeV}$, $\alpha \lesssim 0.1$.

2.2 Total cross-section

More information of interest is the nuclear differential cross-section extrapolated to the forward direction. Using the Optical Theorem and with the usual assumption of spin-independence we can deduce the total cross-section

$$\sigma_t = 4\sqrt{\pi} \hbar \left[\frac{d\sigma}{dt} (t = 0) \right]^{\frac{1}{2}} \sqrt{1 + \alpha^2} \approx 4\sqrt{\pi} \hbar \left[\frac{d\sigma}{dt} (t = 0) \right]^{\frac{1}{2}} \sqrt{(1 + \alpha^2)} .$$

The contributions of the real part are small and they can be easily accounted for by knowing α (if $\alpha \sim 0.1$ the correction to σ_t is only 5×10^{-3}).

The precise determination of σ_t over the energy interval accessible with the ISR, is of considerable interest. Combining σ_t and α measurements one can extend the verification of dispersion relations in the highest energy domain.

Furthermore, Regge models with¹⁶⁾ and without¹⁵⁾ Pomeranchuk trajectory predict substantially different forward cross-sections (Fig. 2). It appears possible to reach a definite experimental evaluation of the nature of the Pomeranchuk amplitude.

2.3 Experimental set-up

The angular range to be explored in order to separate Coulomb and nuclear contributions (Fig. 3) is centered around the value for which $A_{NI}(t) = A_c(t)$. The central angle is easily computed:

ISR energy (each ring)	Angle at which $A_{NI}(t) = A_c(t)$
25 GeV	1.8 mR
15 GeV	3.0 mR
10 GeV	4.5 mR

Assume that two detectors are placed at 6 metres from the interaction point and that they are fully sensitive at 5 mm distance from the standard vacuum chamber; then it is possible to detect with a reasonable efficiency only protons scattered at angles larger than 5 mR (Fig. 4). If both beams are lifted vertically, by one centimetre, it appears possible to reduce the smallest detectable angle to about 3.5 mR. In this way one could determine the angular distribution in the Coulomb interference region only at the lowest energies accessible with the ISR. In order to detect substantially smaller angles, both scattered particles have therefore to be detected beyond the straight section of the interaction region^{*)}. Trajectories

*) We shall assume all the time that the experiment is to be performed in an "even" interaction region where beams are moving inwards.

of scattered particles are shown in Fig. 5. Scatterings in the horizontal plane appear much more favourable for the following reasons:

- i) The available aperture of the machine is much larger (150 mm in the horizontal plane, 50 mm in the vertical plane).
- ii) The maximum displacement (2.68 cm/mr) occurs in a long straight section rather than between the two D magnets of the normal period.

The largest scattering angle for which particles can still be contained inside the magnetic structure is shown in Fig. 6. We assume that both beams are moved radially to the extreme edge of the available aperture, i.e. with the beam centre at 48 mm from the magnet centre (bottom of the stack). This is a conservative value since one could perhaps hope to reduce further locally the allowance for closed orbit distortions.

We propose to increase the available aperture by somewhat enlarging the vacuum chamber, since tolerances on the magnetic-field value and gradient for scattered particles, can be somewhat less severe than the ones imposed by the circulating beam. The ISR pole-profile and field-configuration are shown in Fig. 6. There is no practical limitation in the aperture on the open magnet size. On the closed side, substantial distortions of the field gradient occur beyond about 10 cm from the magnet centre and the field value itself drops below the one of equilibrium orbit ($x = 0$) at about 17 cm from magnet centre. The main limitation in the magnetic aperture (see Fig. 7a) takes place in the second F magnet and it is relative to the proton which is scattered towards the high-field side.

Enlarged vacuum chambers have been designed by the ISR-Vacuum Group for beam ejection and injection. Such chambers permit to extend by about 4 cm the available aperture on the narrow-gap side (Fig. 7b). Scattering angles up to about 6 mr can, therefore, be contained in the four magnets of the ISR period.

Jones³⁾ has originally proposed to introduce counter matrices inside the vacuum chamber in order to detect both diffused particles. It is not obvious that background conditions are such as to permit to operate scintillation counters at about 1 cm distance from a $10^{13} \div 10^{14}$ circulating

protons. Therefore, a much more conservative design is presently proposed. Scattered protons are extracted from the vacuum chamber by septum magnets and focused to a point by additional beam transport elements (Figs. 8 and 9). The focal points are conjugate to the interaction point. The momentum and the scattering angle of the protons are measured by a set of wire spark chambers in front and behind the analyzing magnet B₅. The main parameters of the small angle spectrometer are summarized in Table 1.

Table 1

Parameters of small angle spectrometer

<u>Total length</u> (from interaction point to focus).	60.0 m
<u>Acceptance</u>	
a) horizontal	3.0 mR
b) vertical	±1 mR
<u>Solid angle</u>	6×10^{-6} sterad.
<u>Angular magnification</u>	
a) horizontal plane	1.25
b) vertical plane	1.60
<u>Bending magnets</u>	
a) inside vacuum chamber (septum)	B ₁ , B ₂ 2
b) outside vacuum chamber	B ₃ , B ₄ 2
c) bending magnet	B ₅ 1
<u>Quadrupoles</u>	Q ₁ , Q ₂ 2 × 1.5 m

The parameters of the septum magnets are listed in Table 2.

Table 2

Parameters of septum magnets (ISR design)

	B ₁ ,B ₂	B ₃ ,B ₄
Nominal length	1.0	2.0 m
Gap	3.0	4.0 cm
Useful width	11.0	16.0 cm
Current (for 25 GeV/c)	12×10^3	8×10^3 A
Number of turns	3	6
Septum thickness	1.0	5.0 cm
Magnetic field of nominal current	1.5	1.5 T
Resistance	0.8×10^{-3}	3.2×10^{-3} ohm
Power dissipation (for 25.0 GeV/c)	120.0	210.0 kW
Weight	0.90	4.0 tons
Ultra-vacuum	Yes	No

Magnets B₁, B₂, B₃ and B₄ have been designed by the ISR group for beam ejection and injection. Quadrupoles Q₁ and Q₂ and the bending magnet B₅ are standard PS elements.

Trajectories for scattered particles in the extraction channel are shown in Figs. 10 and 11. The septum magnets B₁, B₂ are inside the vacuum chamber. A thin window separates the rough vacuum in the remaining part of the spectrometer from the ISR vacuum system.

The radial aperture of the septum magnet is sufficient to accommodate an angular interval of about 3 mr. Furthermore, the smallest scattering angle which could be detected is approximately 1 mr (i.e. the septum thickness 1 cm, beam half width 0.8 cm^{*}), safety 0.8 cm).

Therefore we propose to cover the angle interval 1 mr ÷ 6 mr with at least two overlapping intervals, 1 mr ÷ 4 mr and 3 mr ÷ 6 mr. The angle interval could be changed by displacing radially the circulating beam.

*) We assume that some beam "shaving" is done to measure this very small scattering angle (see page 9).

The solid angle accepted by the spectrometer is $\Delta\Omega = 6 \times 10^{-6}$ sterad. With a forward nuclear cross-section $dN/d\Omega$ ($\theta = 0$) $\sim 4 \times 10^4 \text{ int}^{-1} \text{ sr}^{-1}$ we compute

$$N = \frac{dN}{d\Omega} \cdot d\Omega = 4 \times 10^4 \times 6 \times 10^{-6} = 2.4 \times 10^{-3} \text{ int}^{-1}$$

namely about one interaction out of 400 gives a count in the spectrometers due to nuclear scattering alone. Because of the presence of Coulomb scattering in the lowest angle range the counting rate is increased by about an order of magnitude. Therefore:

$$1 \text{ mR} < \theta < 3 \text{ mR} \left\{ \begin{array}{ll} \sim 10 \text{ ev/sec} & \text{for } I = 1\text{A} \\ \sim 1 \text{ ev/sec} & \text{for } I = 330 \text{ mA} \end{array} \right.$$

2.4 Beam parameters. Shaving

In order to be able to observe scattering events at the smallest scattering angles, the beam size must be as reduced as possible.

The optimized "filling" conditions for a given aperture¹⁷⁾ are such that $\frac{2}{3}$ of the space is to be taken by betatron oscillations and $\frac{1}{3}$ by synchrotron oscillations. Let us assume that we require a beam which horizontally has a full width in front of the septum magnets, $\langle x \rangle = 15 \text{ mm}$. At this point the betatron parameters and the momentum compaction are respectively:

$$\beta_H = 38 \text{ m} \quad \beta_V = 12 \text{ m} \quad \alpha_p = 2.3 \text{ m} .$$

A synchrotron width $\Delta x_p = 5.0 \text{ mm}$ gives:

$$\frac{\delta p}{p} = \frac{1}{\alpha_p} \cdot \Delta x_p = 0.2\% ,$$

i.e., $I \sim 2\text{A}$ for the standard parameters of the ISR Study Report.

In order to reduce the full betatron width to 10 mm in the point where $\beta_H = 38 \text{ m}$, a certain amount of beam shaving is necessary. We shall assume that this operation can be performed in the ISR, and therefore no allowance for injection error has been included.

The full betatron width computed at $\beta_H = 38 \text{ m}$ with the parameters of the ISR Study Report is $\langle x \rangle \sim 21.0 \text{ mm}$ (for 25 GeV/c). Therefore, the

beam emittance has to be reduced by the factor $(10/21)^2 = 0.226$ corresponding to $I \sim 0.45$ A for a uniform current density over the beam emittance.

If shaving is performed only in the horizontal plane, the ratio of vertical and horizontal emittances which originally was:

$$\frac{E_H}{E_V} \cong \frac{2}{1} \quad (\text{ISR Design Study Report})$$

becomes

$$\frac{E_H}{E_V} = \frac{1}{2} \quad (\text{p-p scattering after shaving})$$

Therefore, couplings between horizontal and vertical betatron oscillations are expected to be about as important as in the standard beam conditions. If these couplings are in fact important,

$$\frac{E_H}{E_V} \sim 1 \quad \text{and} \quad I \sim 225 \text{ mA} .$$

The values of the current turn out to be adequately large in both cases (more than 1 ev/sec). The effects of scattering on residual gas are important for beams of reduced size. Particle loss due to single Coulomb scattering occurs if a proton is scattered to an angle larger than a value determined by the maximum available horizontal aperture. Furthermore, beam blow-up takes place due to multiple Coulomb scattering. This has two effects:

- i) losses of beam due to aperture limitations;
- ii) reduction of the luminosity due to vertical beam blow-up.

It is intended to keep the horizontal beam size constant by periodic beam shaving operations. Assuming an average pressure of 10^{-3} tor of N_2 or CO we expect an over all decrease of interaction rate of a factor 2 after about 2 hours.

2.5 Detecting apparatus

The trajectories of the scattered particles through the spectrometer are shown in Figs. 10 and 11. Neglecting errors in the magnetic structure, the angle and position of the scattered particle in the interaction region

are uniquely related to the corresponding direction and position at the final double-focal point. The errors caused by current fluctuations and field inhomogeneities due to end effects, saturation and imperfections in the construction contribute to the error in reconstructing the interaction point and scattering angle. The resulting uncertainties have been approximately evaluated and give an over all sum of about 1 to 2 mm. The longitudinal position of the interaction point is badly determined from the geometry alone because of the very small scattering angles. However, time-of-flight measurement between two counters placed in the focus of each of the two spectrometers can be used to determine the position of the interaction point to about 16.6 cm/nanosecond.

We foresee presently four planes of double (x,y) Charpak chambers before and after B_5 magnets in each branch, to determine accurately momentum and direction of each one of the scattered particles (Figs. 10 and 11).

3. THE LARGE ANGLE DETECTOR

3.1 Diffraction region. How far does it shrink?

The angular distribution in the diffraction region is usually parametrized as follows:

$$\frac{d\sigma}{dt}(t) = F(t) \left(\frac{E}{E_0} \right)^{2\alpha(t)-2}$$

The prediction of $\alpha(t)$ for two Regge models^{18,19)} are shown in Figs. 12 and 13. Models are adjusted such as to fit experimental results at present energies. It is foreseen that the shrinkage gradually decreases as the energy increases until the Pomeranchuk limit is reached.

Experimentally, one would like to know up to which energy the diffractive peak is shrinking*).

A very interesting connection between the elastic differential cross-section and the proton electromagnetic form factor $G_E(t)$ was suggested by Wu and Yang²⁰⁾ (1965). The connection can be formulated [Van Hove²¹⁾ (1966)]

*) It seems that at Serpukhov (76 GeV) the angular distribution continues to shrink.

as follows:

$$\left[\frac{d\sigma}{dt} / \frac{d\sigma}{dt} (t = 0) \right] = [G_E(t)]^4$$

Intuitively this is very suggestive because it establishes a relation between nuclear matter density and charge density. Experimentally²¹⁾ the agreement at low momentum transfers is excellent. For larger momentum transfers (see Fig. 14) data suggest that the differential cross-section may shrink with increasing s until the form-factor limit is reached.

3.2 The experimental set-up

Assume that two (x,y) planes of detectors (Charpak chambers) are located at 6.0 and 9.0 metres from the interaction point in each of the two downstream parts of an even interaction region (Fig. 15). Detectors cover all the azimuth and are assumed to be fully sensitive 5 mm away from the vacuum chamber. The computed angular acceptance is shown in Fig. 4. Protons scattered at angles larger than about 5 mr are detected with a reasonable efficiency.

In order to somewhat extend the angle range, both beams could be lifted vertically to bring the beam close to one part of the detector. If it is possible to displace vertically the beams by 1 centimetre, the minimum useful angle is reduced to about 3.5 mr.

For the smaller angles the actual detection efficiency depends somewhat from the geometry. The distribution of the beam-beam interactions can be determined either from:

- i) larger angle scattering events where the detection efficiency is 100% or
- ii) folding-in individual beam distributions determined from beam-gas interaction (Section 4).

Colinearity of the two scattered particles is a valid constraint in order to discriminate against inelastic events. However, at large scattering angles this requirement alone is insufficient to discriminate the very few elastically scattered protons from the much broader angular distribution of other particles produced, mostly soft pions. The effect is elucidated in Table 3. The expected yield of elastically scattered protons is compared with total particle production yields of the thermodynamic model.

Table 3

Elastically scattered protons and secondary particle production at 25 + 25 GeV

θ (mrad)	t (GeV ²)	$\frac{d\sigma}{d\Omega} / \frac{d\sigma}{d\Omega} (t = 0)$ protons	$\frac{dN}{d\Omega} / \frac{dN}{d\Omega} (\theta = 0)$ all charged particles
10	0.0625	0.5	0.71
20	0.25	10^{-1}	0.51
30	0.57	10^{-3}	0.37
50	1.56	10^{-4}	0.21
80	4.0	4×10^{-7}	0.08

There are two independent ways of improving the discrimination against inelastic events:

- i) an anticounter shield as tight as possible is arranged around the interaction volume, in order to reject events in which additional particles are detected. This method is expected to be very efficient at least for large (charged) multiplicity events;
- ii) magnetic analysis is performed on both scattered particles.

We would like to make use of both the anticoincidence and of the magnetic analysis for scattering angles larger than about 20 mr. Several different magnetic field arrangements are possible. We have considered in detail two similar schemes in which no perturbation is induced on the circulating beams.

The choice between the two schemes will be made at a later stage.

3.3 The twin septum magnet

A first scheme is shown in Fig. 16. The magnetic field is oriented in opposite directions in the two gaps and the flux is closed through the iron return pieces. The septum thickness is a compromise between power dissipation and thickness. The main parameters of the magnet are listed in Table 4.

Table 4

Parameters of the twin septum magnet

Nominal magnetic field	1.2 T
Nominal length	2.0 m
Ampere \times turns at nominal field	2.8×10^5
Power dissipation	~ 870 kW
Iron weight	18 tons
Copper weight	4.5 tons
Gap height	28.0 cm
Gap width (each)	35.0 cm

3.4 Alternative magnet design. The twin picture-frame magnet

A second magnet design is shown in Fig. 17. The idea is to embed the vacuum chamber of the ISR in an iron plate which acts as a magnetic shield. The field inside the hole is uniform and only a few gauss if the field is low enough not to saturate the iron. A special insertion of high permeability and high saturation material could help in raising the magnetic field a little higher.

The main advantage of the present design over the double septum is a lower power dissipation in the coils. The choice between the two magnets will be done after more elaborate model work.

3.5 The counter arrangement

The experimental arrangement at the ISR is shown in Fig. 18. Two groups of wire chambers (Charpak) in front (W_1, W_2) and two groups behind (W_3, W_4) the magnet are used to determine the scattering angle and the particle momentum. The position of the magnet and of the wire chambers W_2 and W_3 can be changed according to the angular range which is to be explored. The precision expected on 25 GeV particles is also indicated assuming a ± 0.3 mm accuracy in each chamber plane. The momentum of outgoing particles can be determined to better than 0.4% for most of the positions of the analyzing magnet ($2 \text{ m} < L < 5.5 \text{ m}$).

In order to achieve a reasonable counting rate at larger angles, it is necessary to increase the circulating current within the

available aperture. The momentum uncertainties in the circulating beams $(\Delta p/p)_{\text{beam}}$ are then determined by the width of the betatron oscillation $\langle \Delta X \rangle$ and the momentum compaction α_p , since the interaction point can be accurately reconstructed:

$$\left(\frac{\Delta p}{p}\right)_{\text{beam}} = \frac{1}{\alpha_p} \langle \Delta X \rangle = \frac{1}{230} \langle 1.0 \rangle = 5 \times 10^{-3}$$

This value is well matched to the momentum resolution of the spectrometer magnet.

It is foreseen that groups of wires in the Charpak chambers are selecting the large momentum particles entering the detector. Extensive use of integrated circuits is foreseen in the building of the logics. Only potential candidates are then transferred to a tape by a small on-line computer.

4. DETERMINATION OF THE PARAMETERS OF STORED BEAMS

4.1 Method

In order to determine the detection efficiency and the true scattering angle of small angle scattering events it is necessary to determine exactly the distribution of the circulating protons in angle and space.

We intend to measure these parameters observing elastic scattering events of protons on the residual hydrogen gas in the vacuum chamber^{*)}. Since the forward scattered protons on gas have kinematics and angular distribution very similar to the beam-beam elastic scatterings, this measurement can be carried out simultaneously during the main experiment, recording in addition coincidences between a proton in the forward telescope and the recoil proton at about 90° (see Fig. 19).

The relevant kinematical curves are shown in Fig. 20. The incident proton momentum is fixed to 25.0 GeV/c. The correspondence between the proton angles in the forward direction θ and the recoil angle θ_R is shown. The kinetic energy of the proton recoil T_{pr} increases very rapidly when θ_R departs from 90°. This relation is very slowly dependent on the incident proton momentum K . This is evidenced by the expression:

*) H_2 is expected to be the main constituent of the residual gas.

$$p_R = 2\beta M_p \frac{\cos(\theta_R)}{1 - \beta^2 \cos^2 \theta_R}$$

where

$$\beta = \frac{K}{\sqrt{K^2 + M_p^2}}$$

is the velocity of the centre-of-mass, p_R is the laboratory momentum of the recoil proton of mass M_p .

The curve $\theta(\theta_R)$ is very insensitive to changes of θ_R . At the limit $\theta \rightarrow 0$, we get:

$$\frac{d\theta_R}{d\theta} = \frac{1}{\gamma^2} = \frac{1}{\sqrt{1 - \beta^2}}$$

For $K = 25.0$ GeV/c, $\gamma^2 = 13.7$; for $K = 10$ GeV/c, $\gamma^2 = 6$.

Therefore the recoil proton can be used as a "lever" arm to predict the direction of the forward emitted proton. Observing both diffused particles can be used to predict incident proton direction about to the accuracy with which the forward emitted proton is measured. The point of the interaction vertex can be determined very conveniently from the large opening V of the event.

REFERENCES

- 1) L.W. Jones and B. de Raad, CERN Internal Report AR/Int. SG/62-11, 3 September, 1962, p.11.1.
- 2) B. de Raad, CERN Internal Report AR/Int. SG/62-12, 21 September, 1962.
- 3) L.W. Jones, BNL Report 7534, p.253, 1963.
- 4) K.M. Terwilliger, BNL Report 7534, p.238, 1963.
- 5) A. Minten, CERN Internal Report D.Ph.II/AM/dmh, 13 February, 1968.
- 6) L. di Lella, Contribution to the ISR User's Meeting, CERN, Geneva, 10-11 June, 1968.
- 7) G. Cocconi, CERN Internal Report NP/67/436/mk/5.
- 8) U. Amaldi, Jr., G. Matthiae and P. Strolin, proposal to the ISRC, 10 February, 1969.
- 9) C. Rubbia and P. Darriulat, CERN Internal Note on "High beta interaction region: a magnifying lens for very small angle proton-proton scattering", 1968.
- 10) P. Darriulat and C. Rubbia, CERN Internal Report 68/340/5 SIS/si, 28 February, 1968.
C. Rubbia, Contribution to the ISR User's meeting, CERN, Geneva, 10-11 June, 1968.
- 11) S. Van der Meer, CERN Internal Report ISR-PO/68-31.
- 12) J. Steinberger, "Suggestions for the luminosity measurement of the ISR", June, 1968.
A.P. Onuchin, NP Internal Report 68-26, 14 August, 1968.
- 13) V. Barger, Proc. Topical Conf. on High-Energy Collisions of Hadrons, CERN, January, 1968, p.3.
- 14) P. Söding, Phys. Letters 14, 285 (1964).
- 15) N. Cabibbo, L. Horwitz, J.J.J. Kokkedee and Y. Ne'eman, Nuovo Cimento 45 A, 275 (1966).
- 16) V. Barger, M. Olsson and K.V.L. Sarma, Phys. Rev. 147, 1115 (1966).
- 17) CERN Internal Report AR/Int. SG/64-9, 12 May, 1964.
- 18) C.B. Chiu, S.Y. Chu and L.L. Wang, Phys. Rev. 161, 1563 (1967).
- 19) W. Rarita, R.J. Riddell, Jr., C.B. Chiu and R.J.N. Phillips, UCRL Report 17523 (1967).

- 20) T.T. Wu and C.N. Yang, Phys. Rev. 137 B, 708 (1965).
- 21) L. Van Hove, in Proceedings of the Stony Brook Conference on High-Energy Two-Body Reactions (SUNY, 1966).
J.J.J. Kokkedee and L. Van Hove, Nuovo Cimento 42, 711 (1966).

Figure captions

- Fig. 1 : Experimental values of the parameter $\alpha = \text{Re}(A_N)/\text{Im}(A_n)$ are compared with the results of the calculations of Refs. 14, 15 and 16.
- Fig. 2 : Forward scattering elastic p-p cross-section as deduced from the calculations of Refs. 15 and 16 versus the laboratory momentum of the incident proton on a stationary target. The corresponding momentum range for the ISR is indicated.
- Fig. 3 : Differential p-p elastic scattering cross-section as a function of the scattering angle θ for 25 GeV/c and 10 GeV/c intersecting beams.
- Fig. 4 : Geometric detection efficiency as a function of the scattering angle for a system of counters located outside the vacuum pipe, 6 m from the interaction point.
- Fig. 5 : Trajectories of protons scattered at various angles, followed through the magnetic fields of the ISR magnets.
- Fig. 6 : Trajectories of protons scattered at various angles, followed through the magnetic fields of the ISR magnet. The beam has been displaced and the vacuum chamber enlarged in order to accept scattering angles as large as possible.
- Fig. 7a : Configuration of the magnetic field in the median plane of an ISR magnet as a function of the distance from the beam line.
- Fig. 7b : Cross-section of a standard and of an enlarged vacuum chamber in an ISR magnet gap. The enlarged vacuum chamber is of the type designed for injection.

- Fig. 8 : Schematic arrangement of the upstream part of the very small angle spectrometer. B1 and B2 are injection type septum magnets. B3 and B4 are separated from the ultra vacuum region by a thin window.
- Fig. 9a : Plan view of the left branch of the very small angle spectrometer. The yoke of the first D magnet has to be reversed.
- Fig. 9b : Plan view of the right branch of the very small angle spectrometer. The yoke of the first F magnet has to be reversed.
- Fig. 10 : Optical properties of the very small angle spectrometer in the horizontal plane. The trajectories of a 2.5 mr and of a 5.5 mr scattered protons are followed from the interaction point to the spectrometer focus. Also shown are the acceptance limitations due to vacuum chambers and magnet gaps.
- Fig. 11 : Optical properties of the very small angle spectrometer in the vertical plane. The trajectories of a 0.5 mr and of a 1.0 mr scattered protons are followed from the interaction point to the spectrometer focus. Also shown are the acceptance limitations due to vacuum chambers and magnet gaps.
- Fig. 12 : The variation with t of the parameter $\alpha(t)$, as predicted from the calculation of Ref. 18. The curves are labelled with the incident proton momentum.
- Fig. 13 : The variation with t of the parameter $\alpha(t)$, as predicted from the calculation of Ref. 19 (solution 3). The curves are labelled with the incident proton momentum.
- Fig. 14 : Plot of $\left[\frac{d\sigma/dt}{(d\sigma/dt)_{t=0}} \right]$ versus laboratory momentum at fixed t . The $\left[\frac{G_E^P(t)}{G_E^P(0)} \right]$ values are shown for comparison.

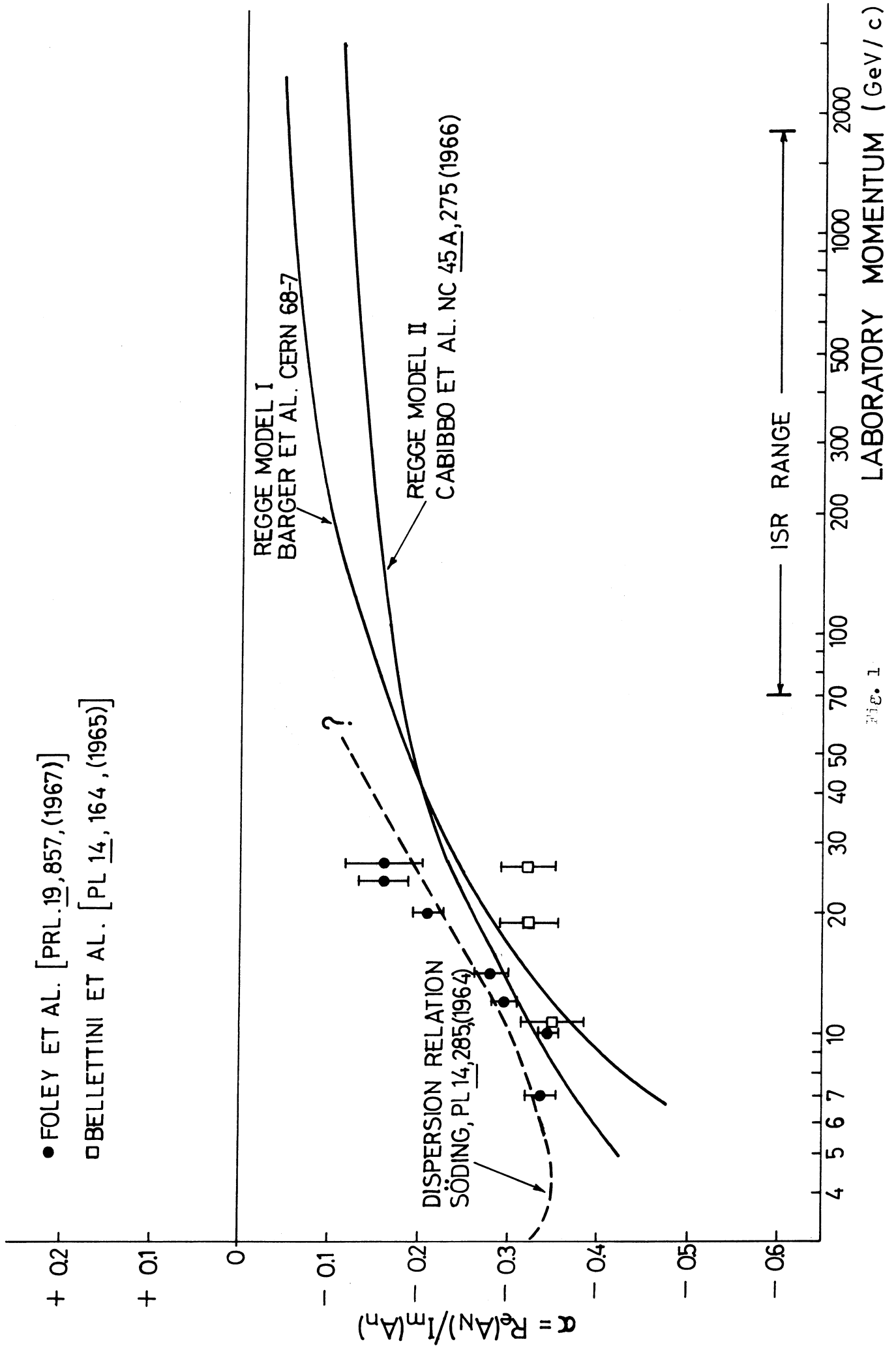


Fig. 1

FORWARD SCATTERING CROSS SECTION

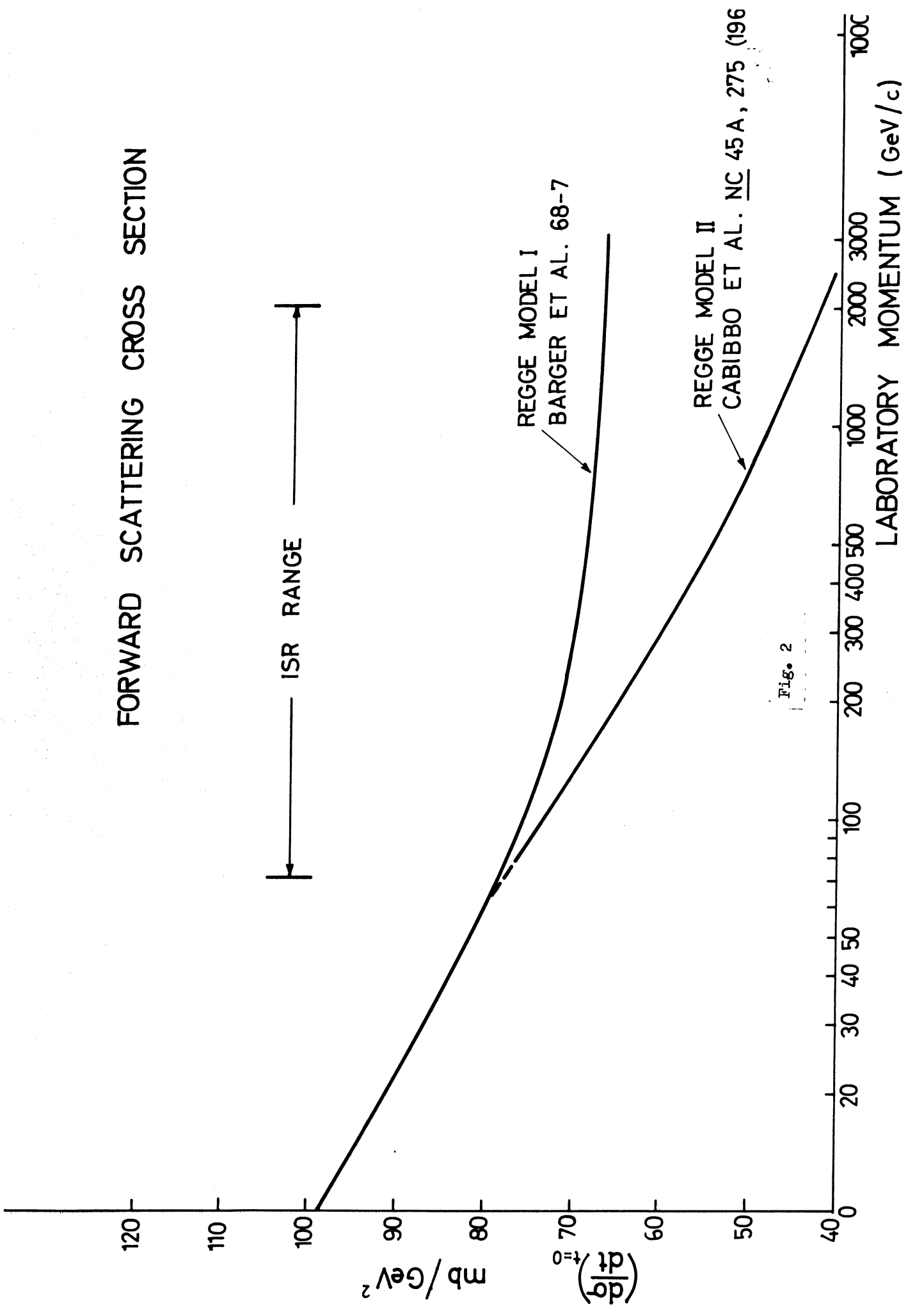


Fig. 2

ELASTIC PROTON - PROTON
SCATTERING AT ISR
(NO REAL PART IN NUCLEAR
SCATTERING AMPLITUDE)

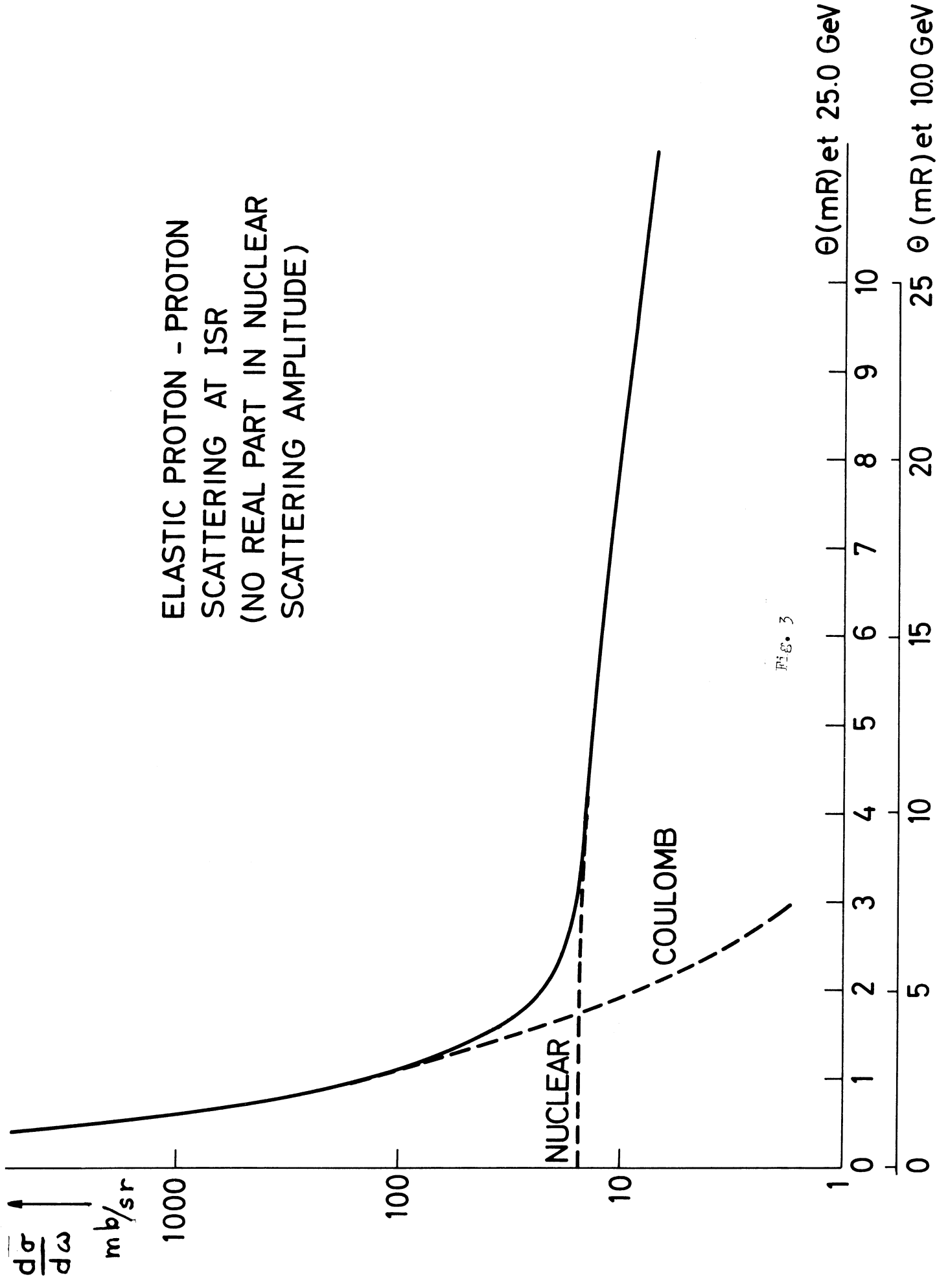


FIG. 3

GEOMETRICAL DETECTION EFFICIENCY VS SCATTERING ANGLE
(LARGE ANGLE DETECTOR)

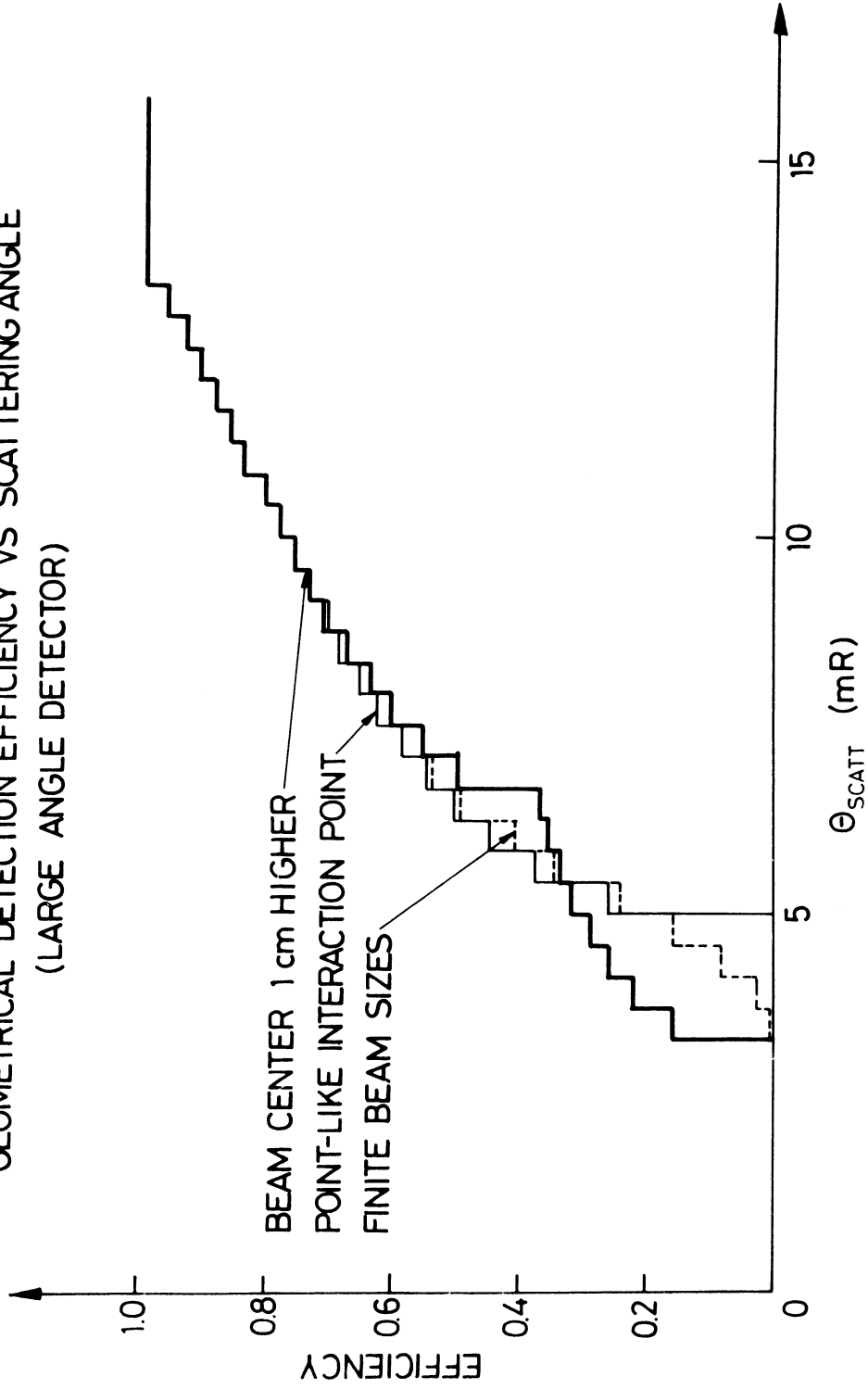


FIG. 4

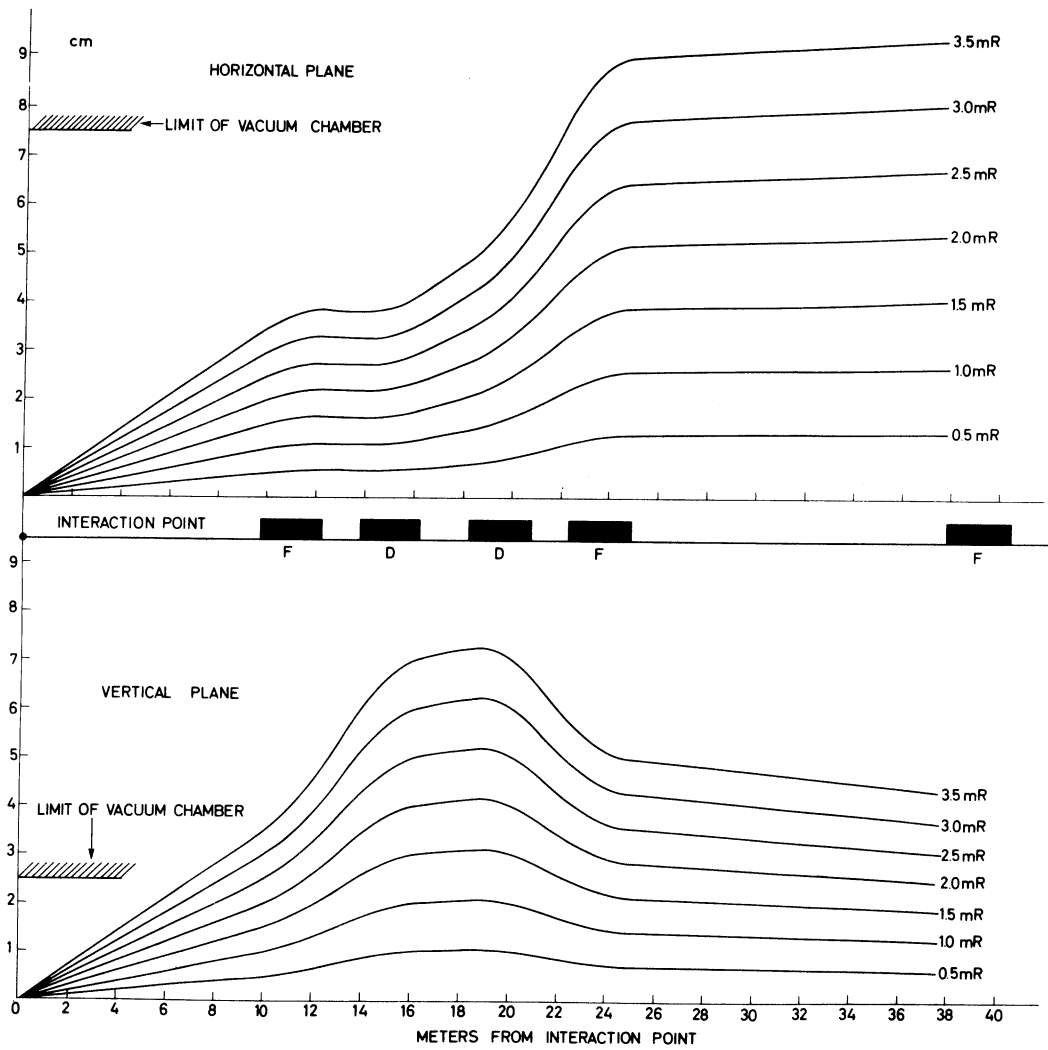
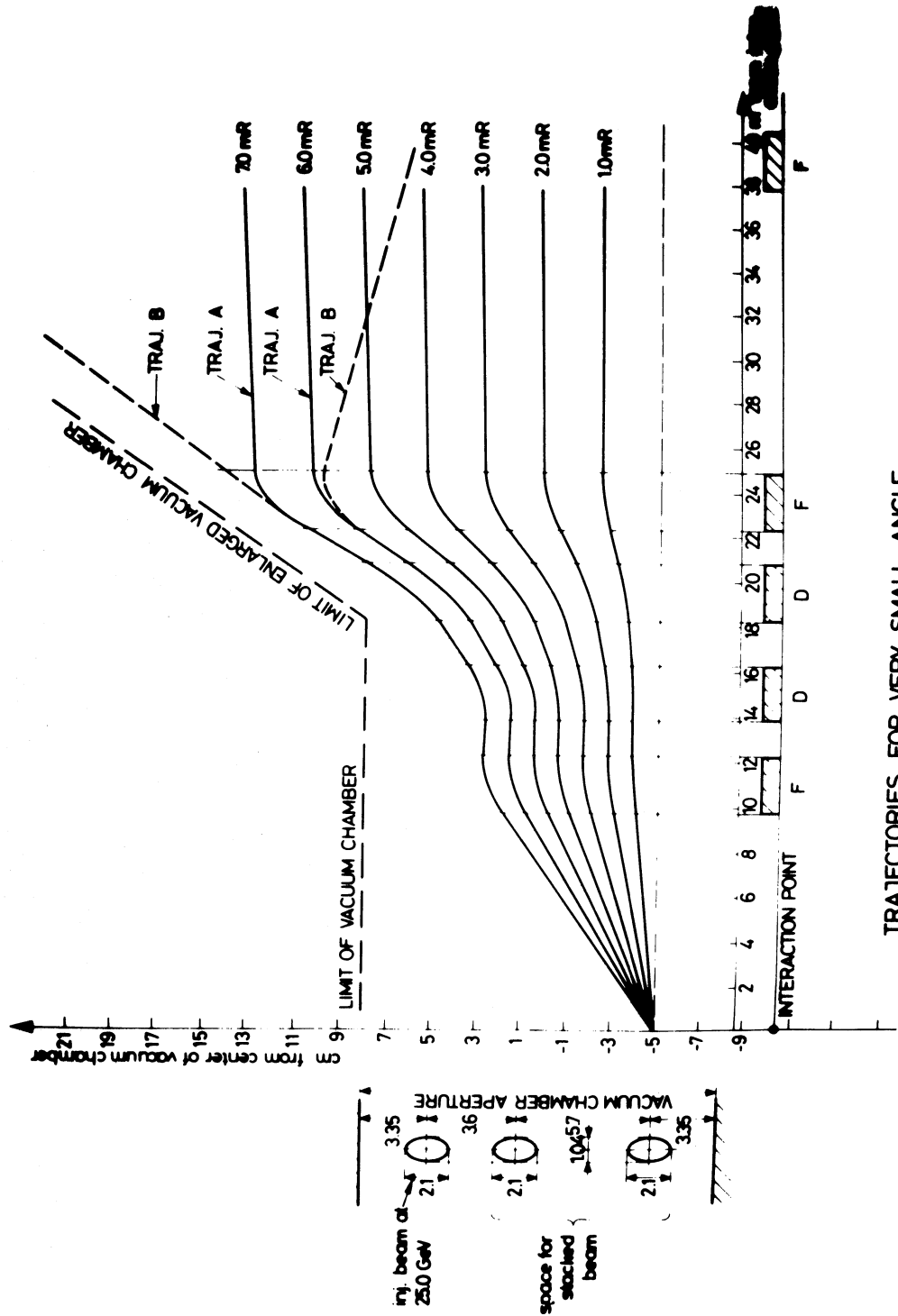


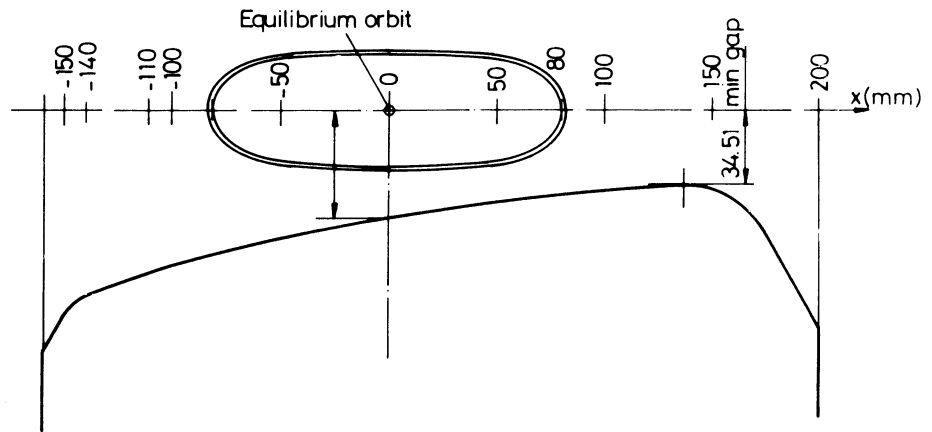
Fig. 5



TRAJECTORIES FOR VERY SMALL ANGLE
PROTON - PROTON SCATTERING

Fig. 6

ISR POLE PROFILE AND FIELD CONFIGURATION



$B_0 = 5000$ GAUSS

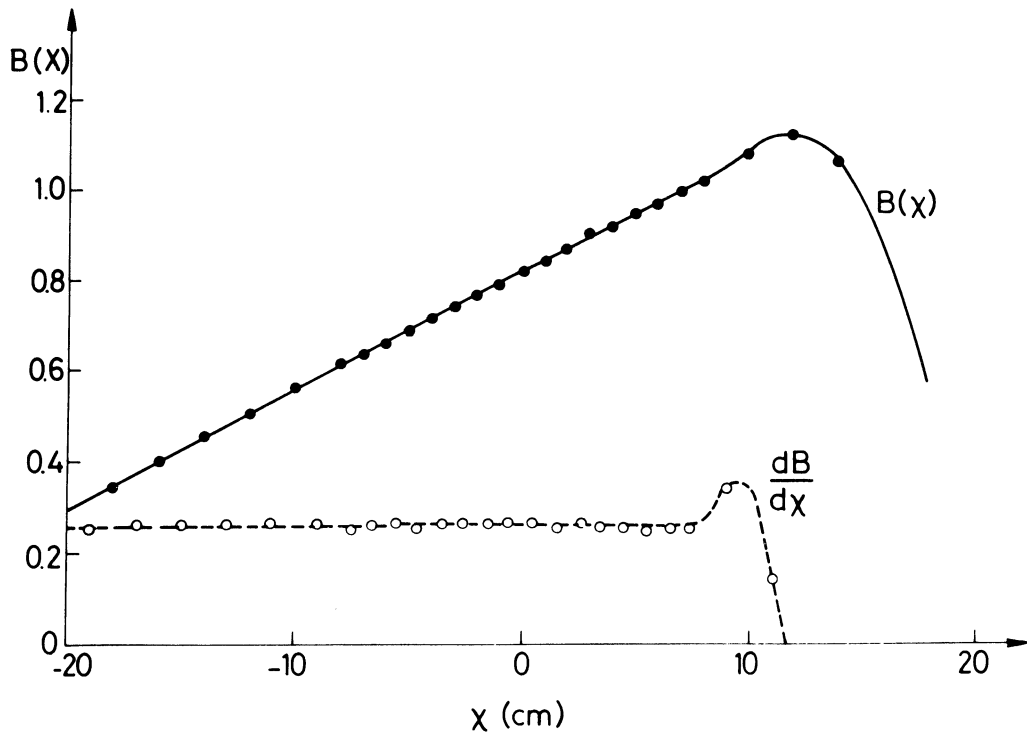


Fig. 7a

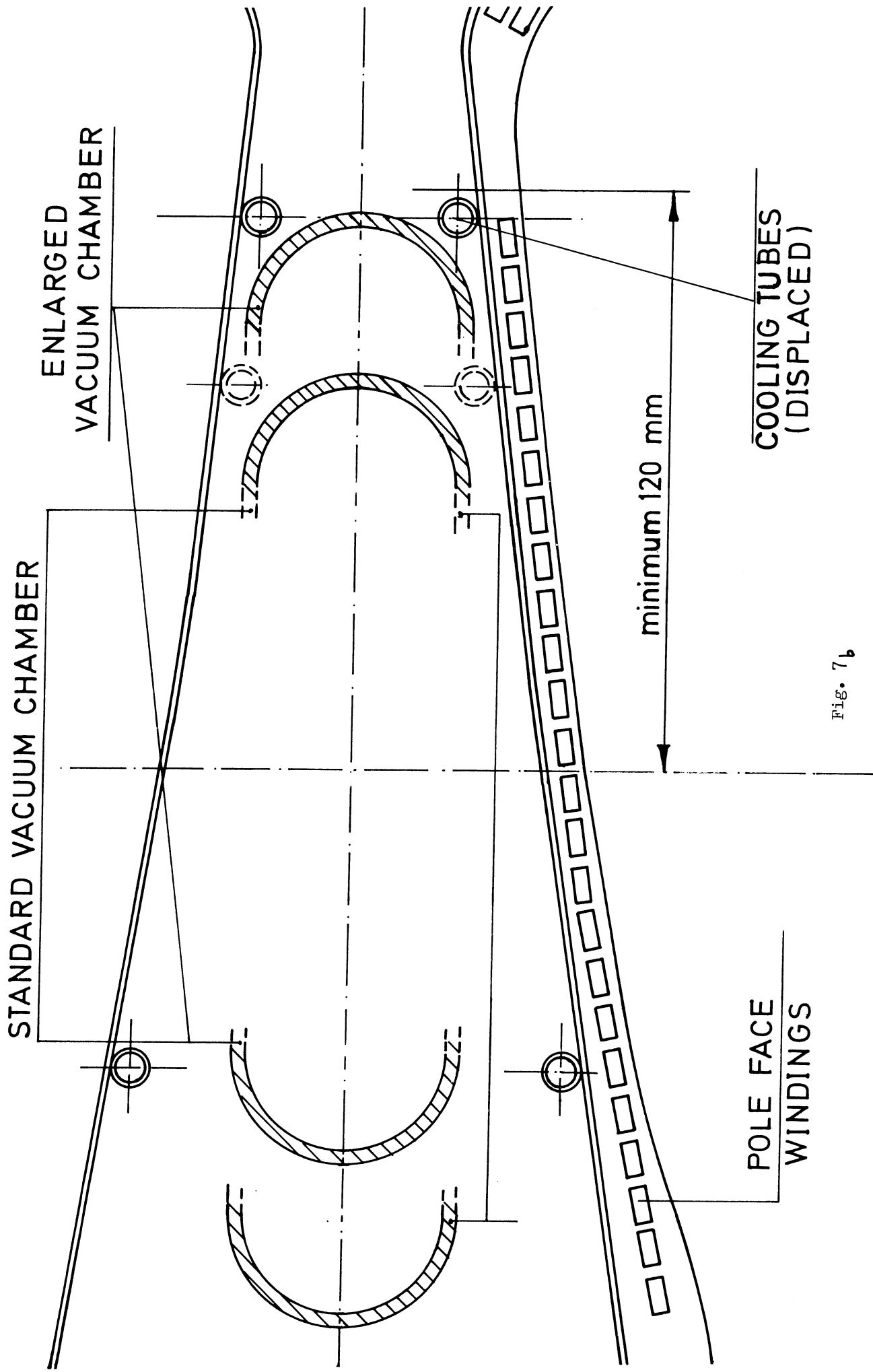


Fig. 7b

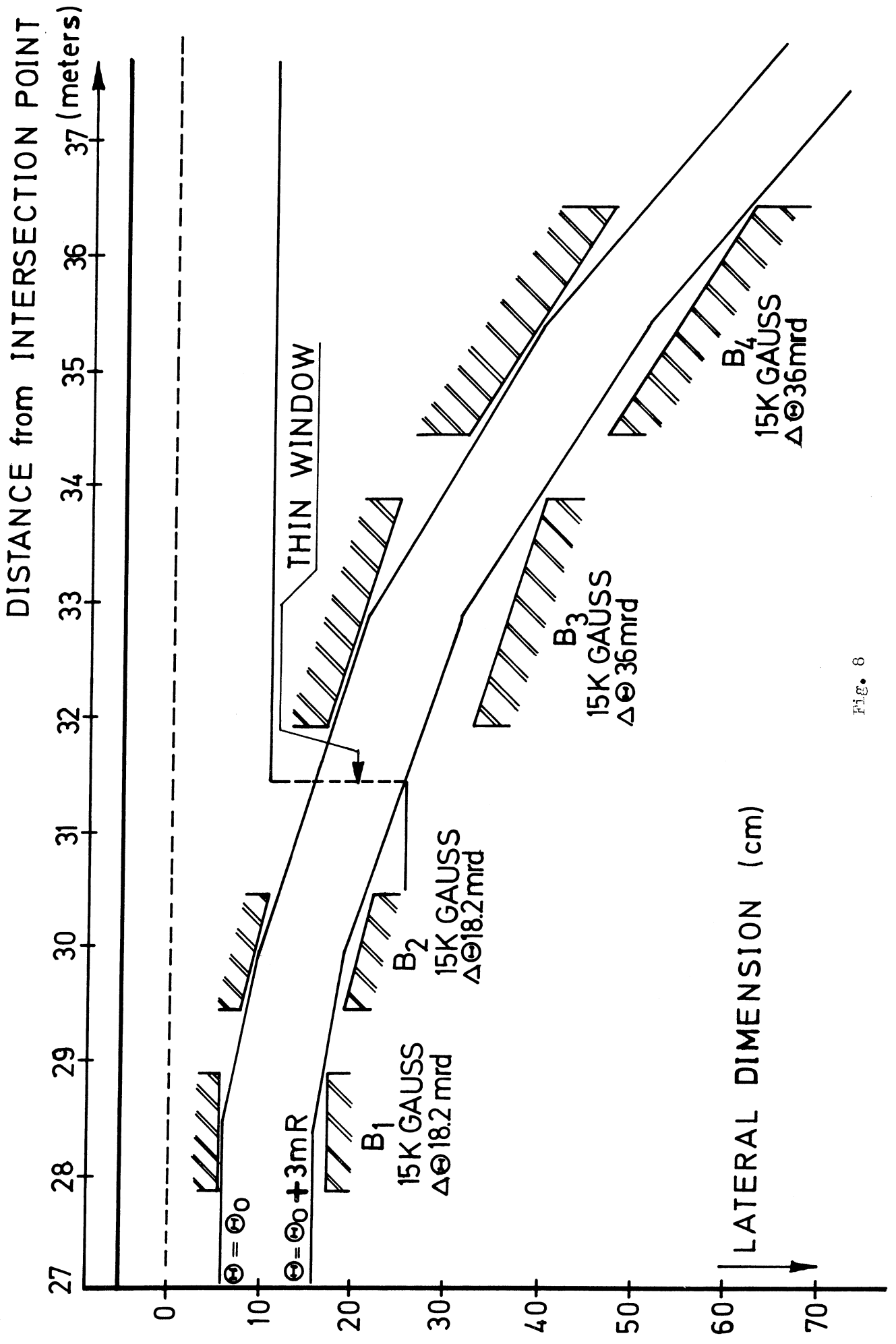


FIG. 8

B: bending magnets
 Q: quadrupoles
 W: wire counters

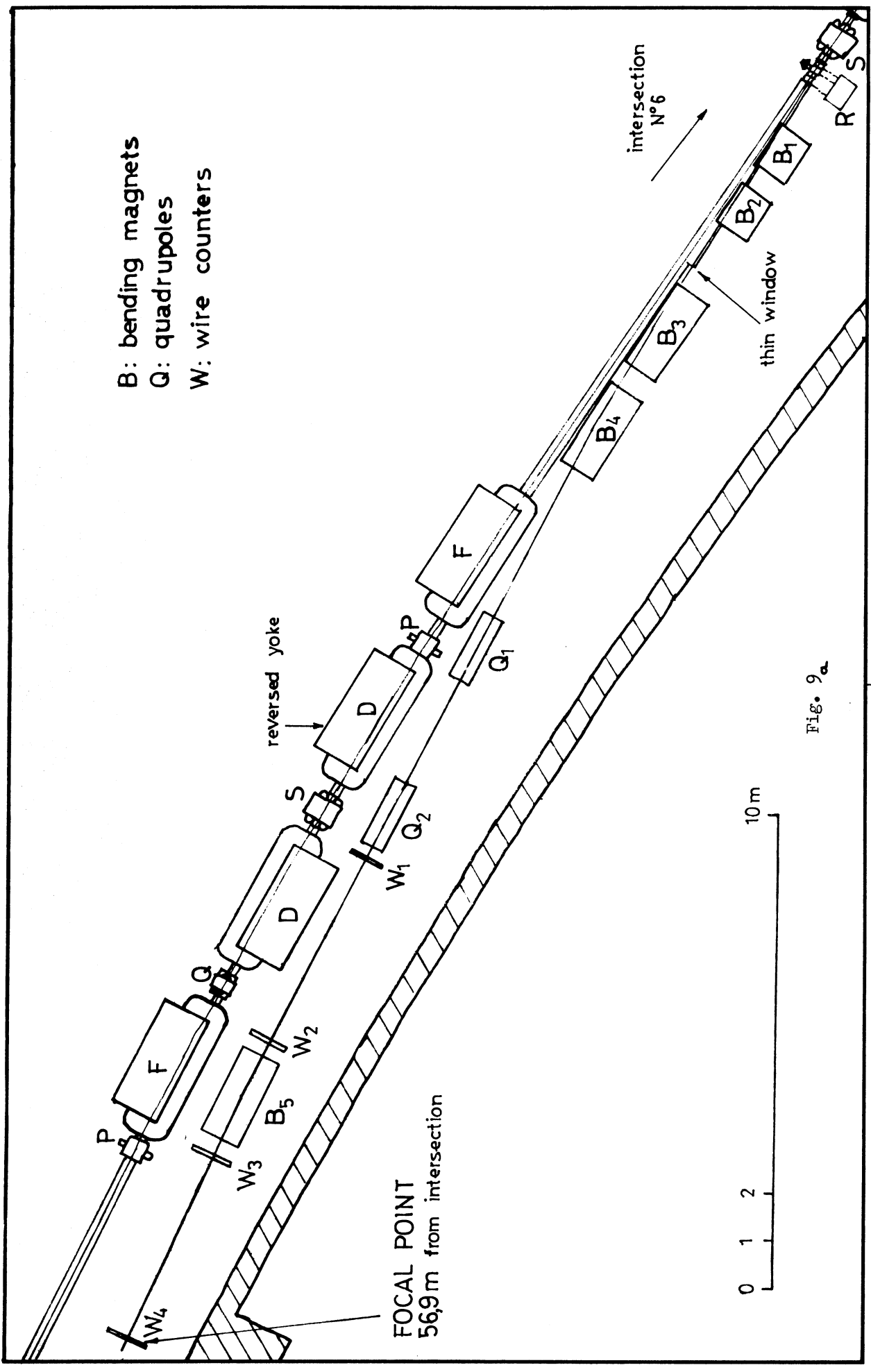


FIG. 9_a

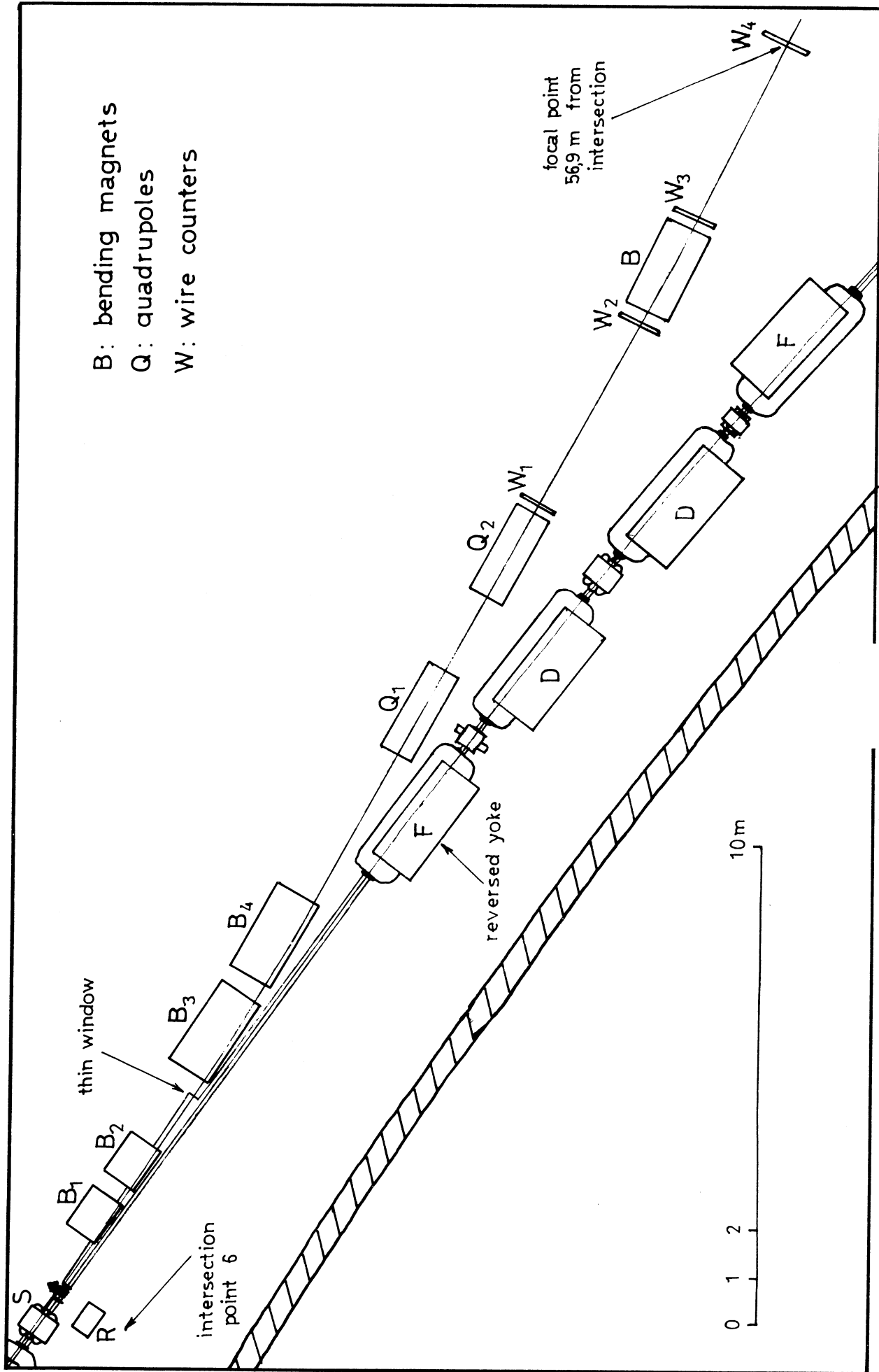


Fig. 9b

HORIZONTAL PLANE

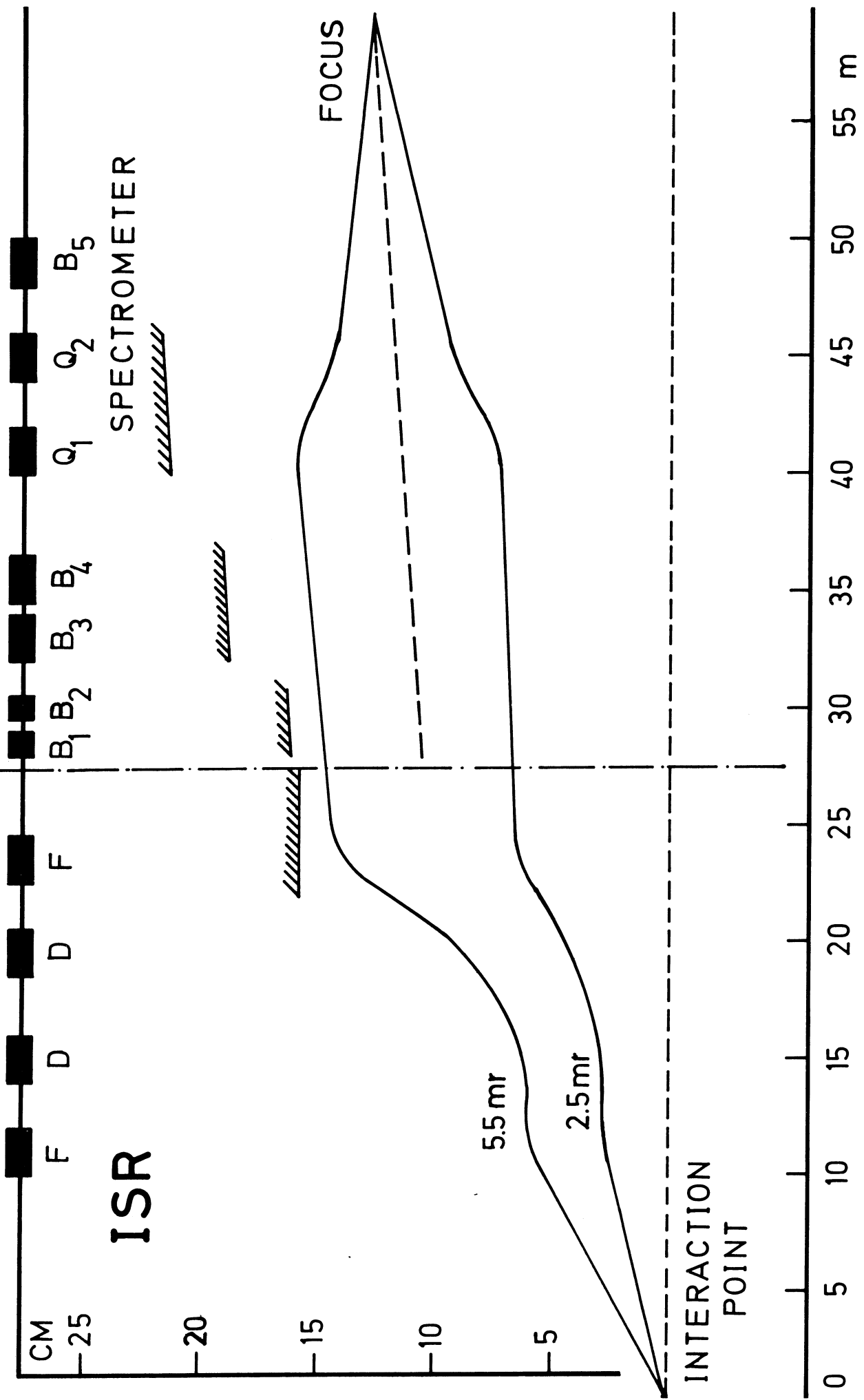


Fig. 10

VERTICAL PLANE

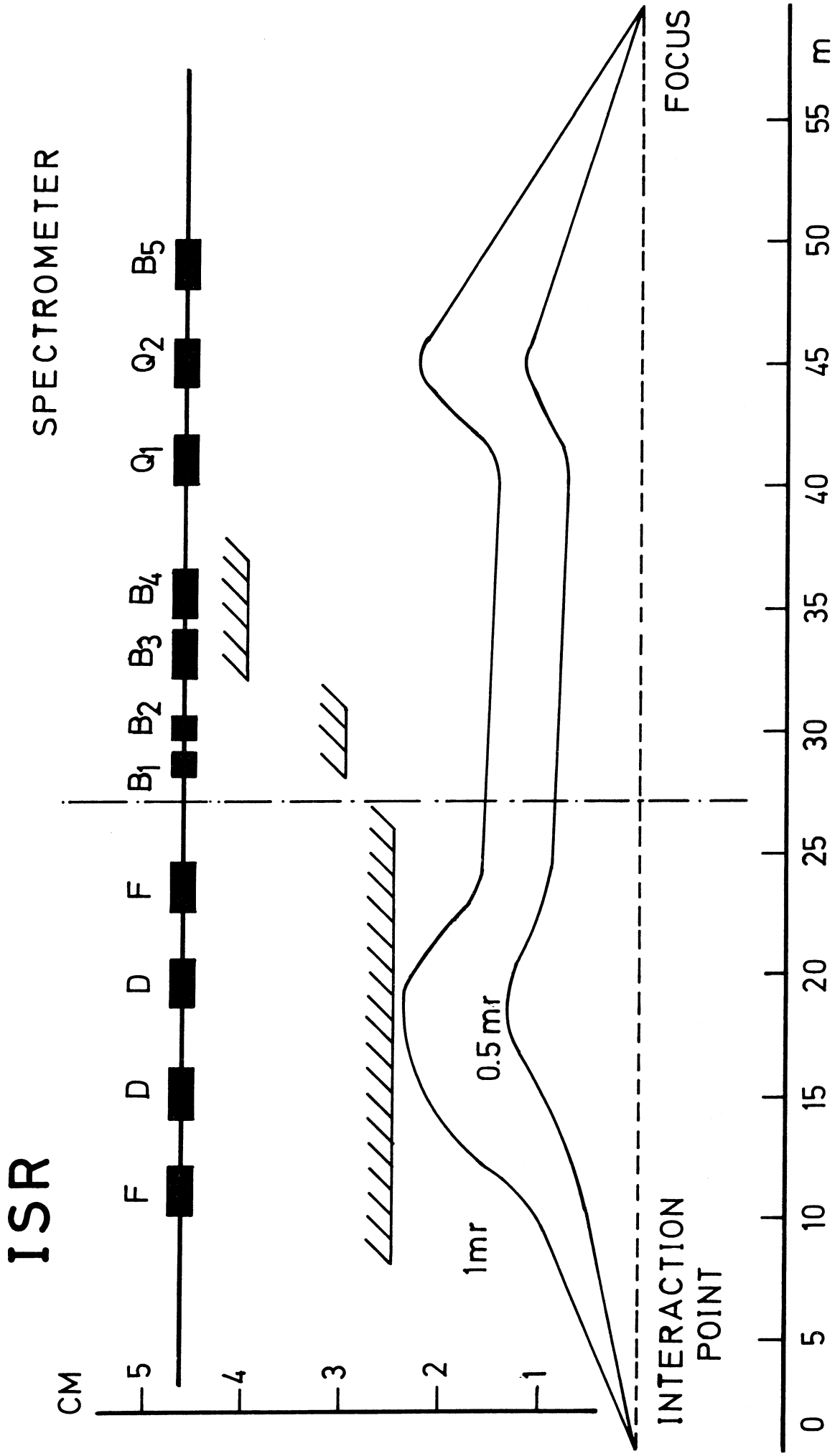


FIG. 11

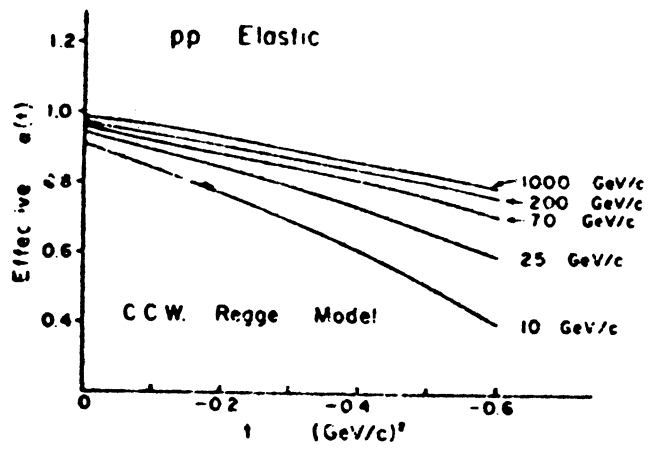
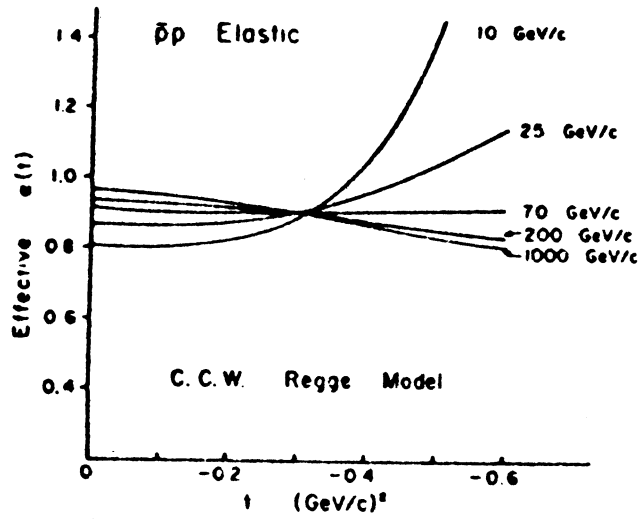


Fig. 12

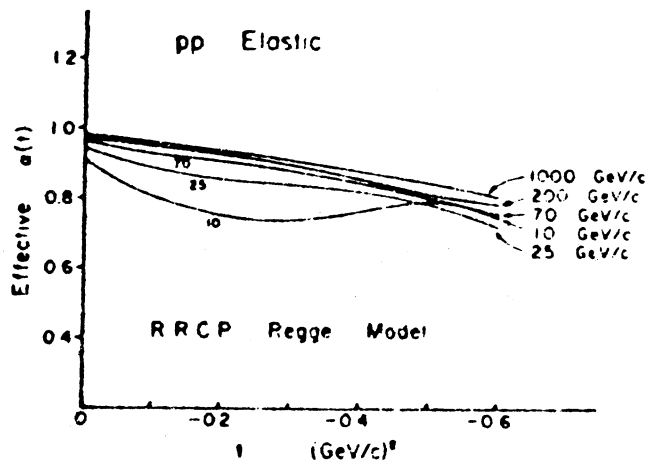
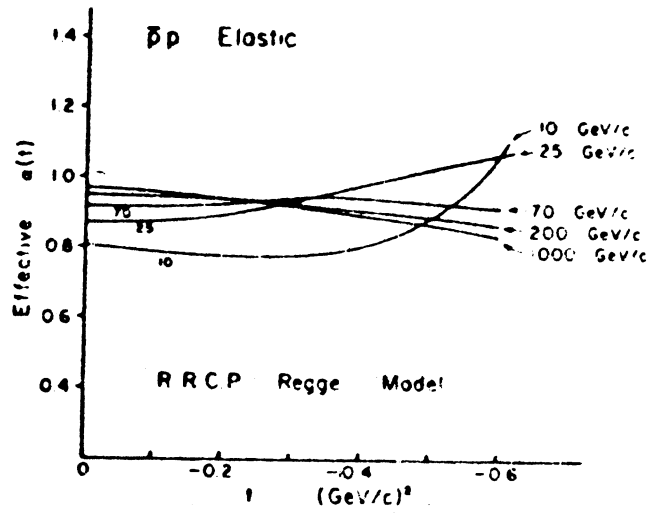


Fig. 13

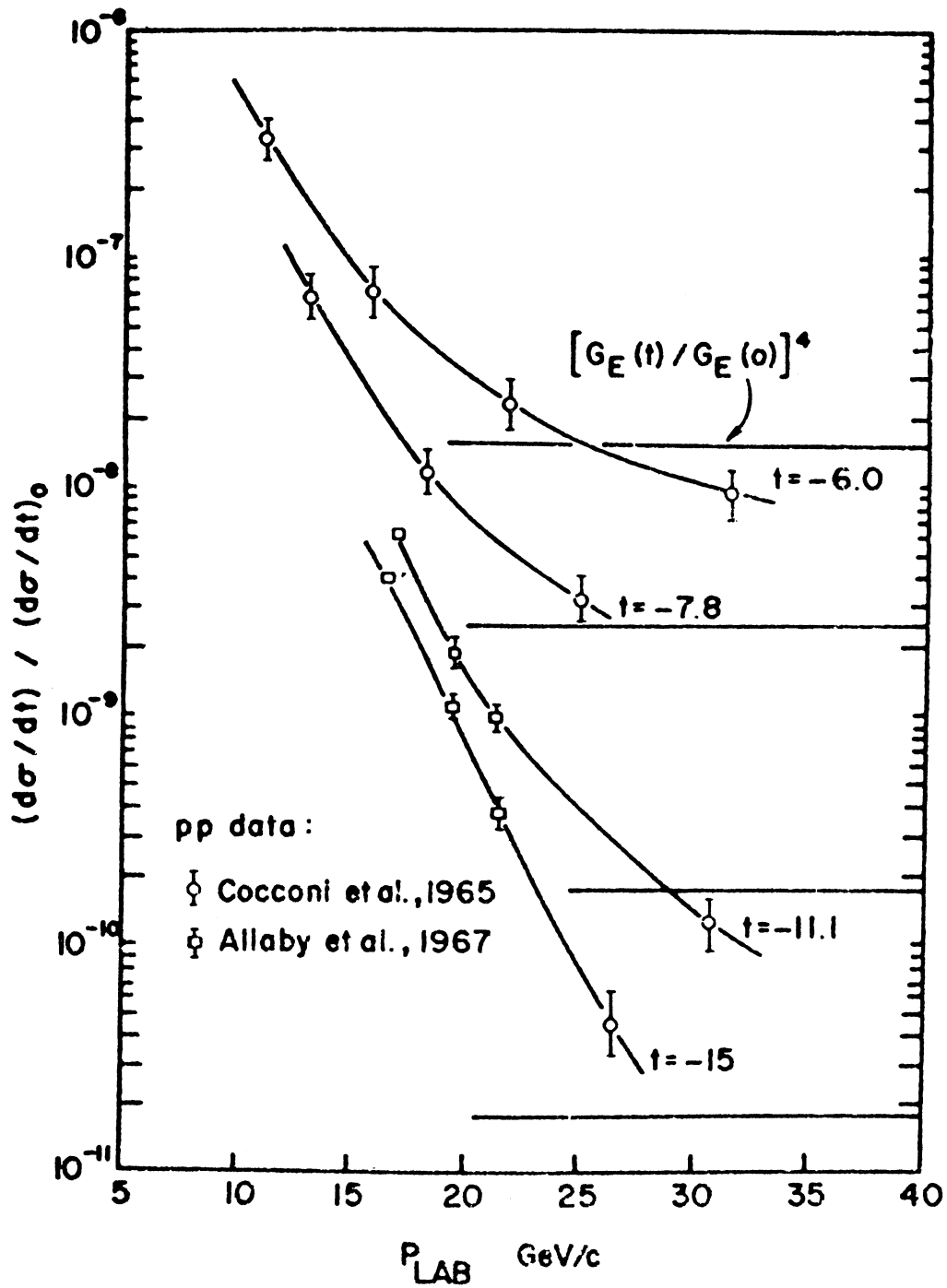


Fig. 14

**MEDIUM AND LARGE ANGLE
PROTON-PROTON SCATTERING**

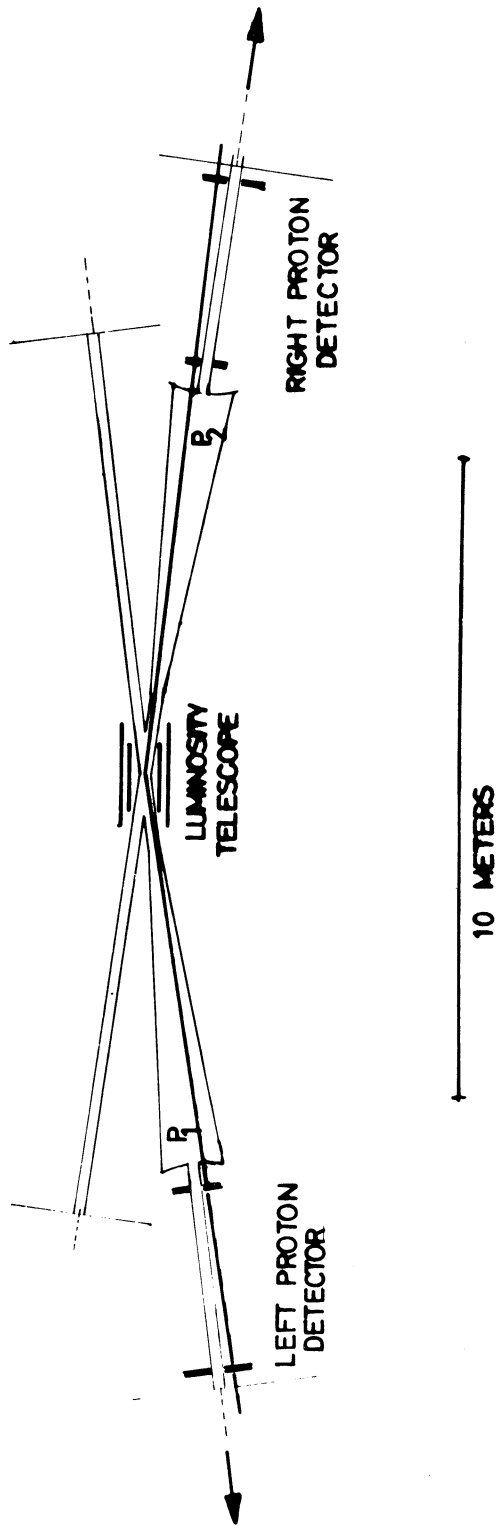
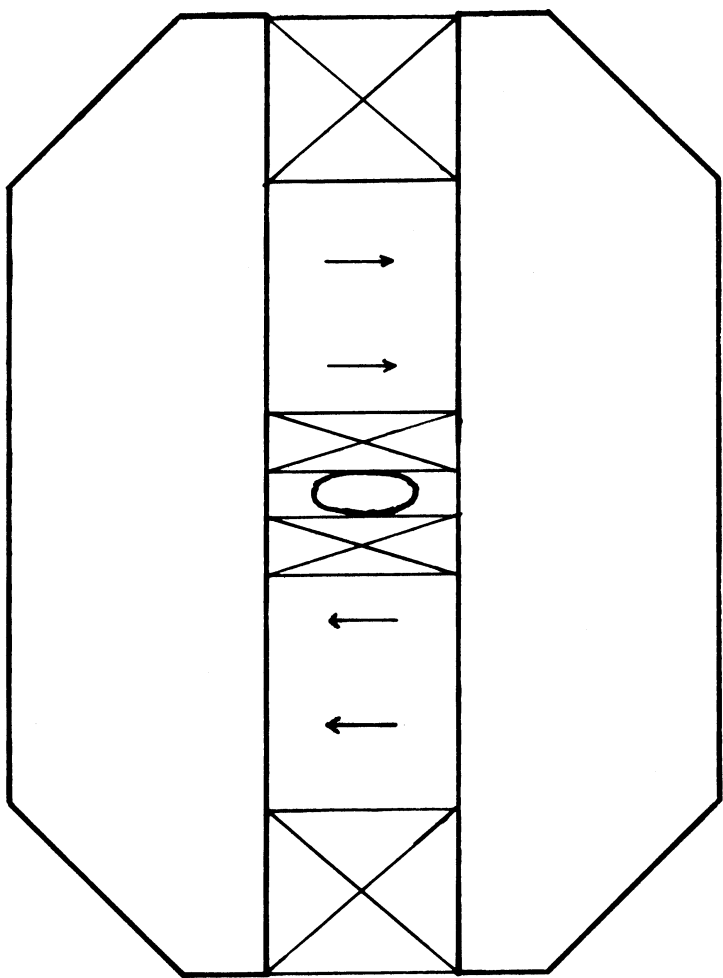


Fig. 15

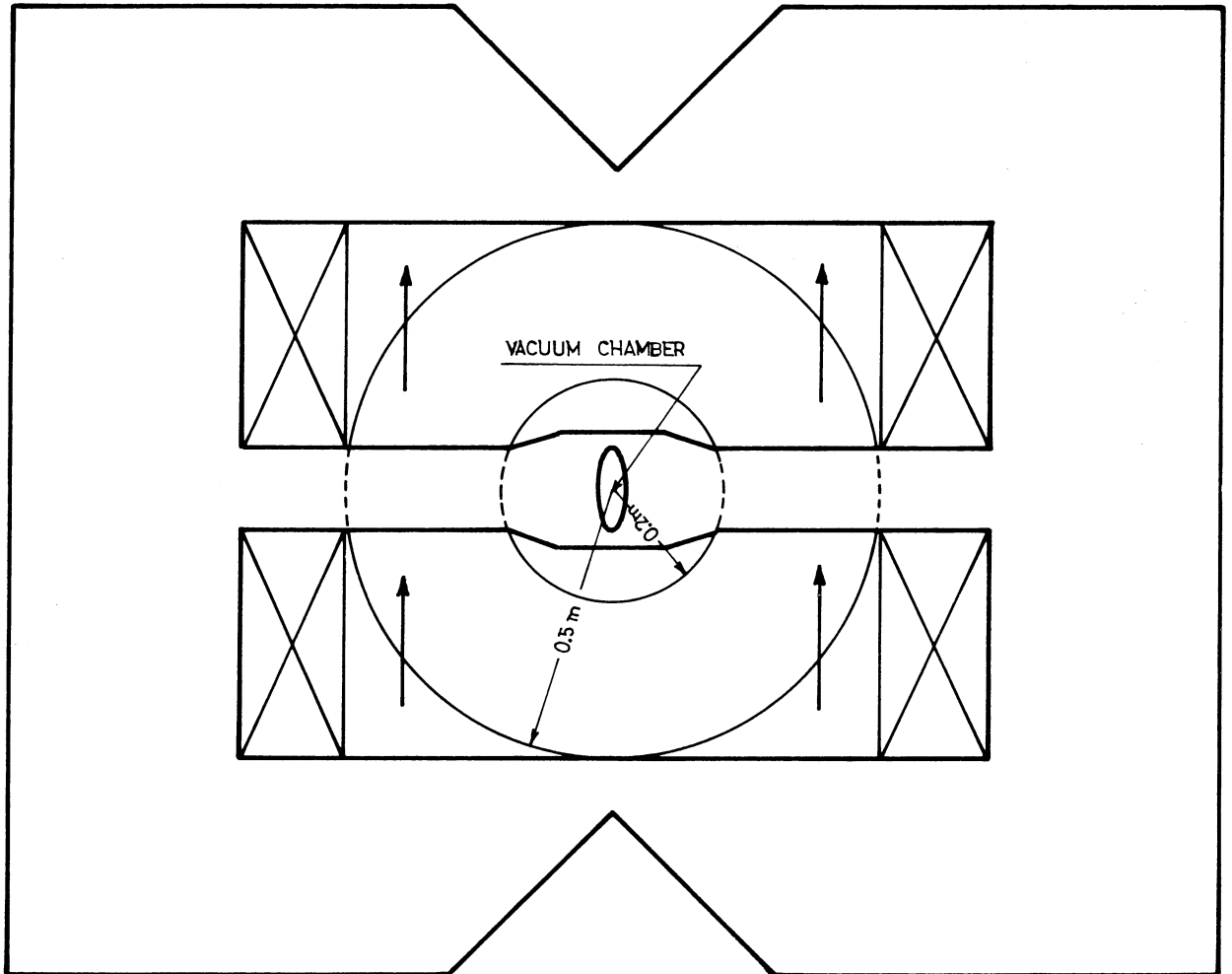
TWIN SEPTUM MAGNET



50 cm

Fig. 16

TWIN PICTURE FRAME MAGNET



Iron : 43 tons for 2 m length

Copper : 5.7 tons " " "

$B_0 = 1.2$ T

0 0.1 1m

Fig. 17

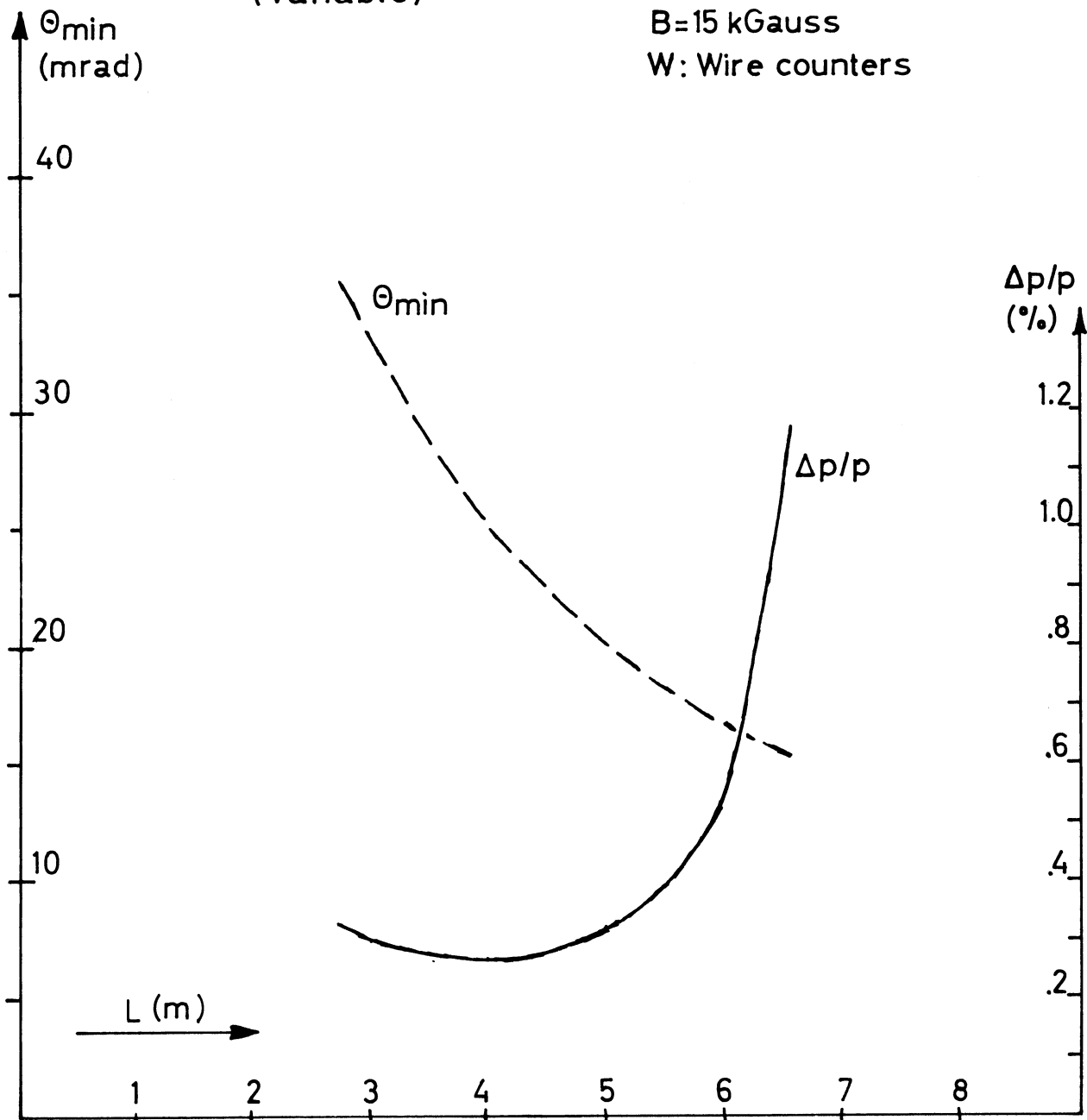
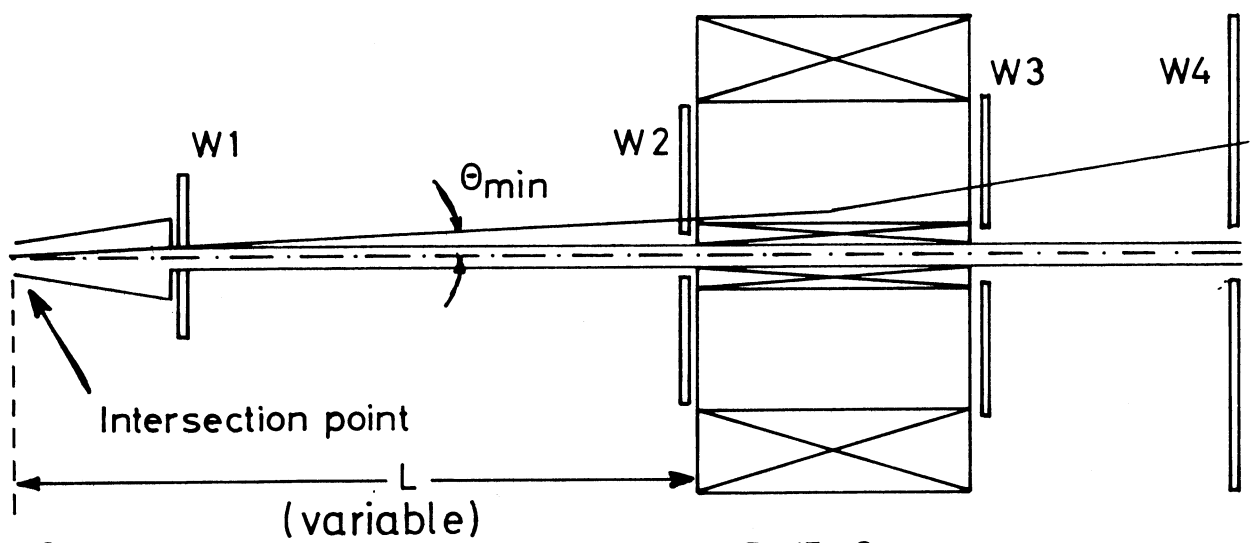


Fig. 18

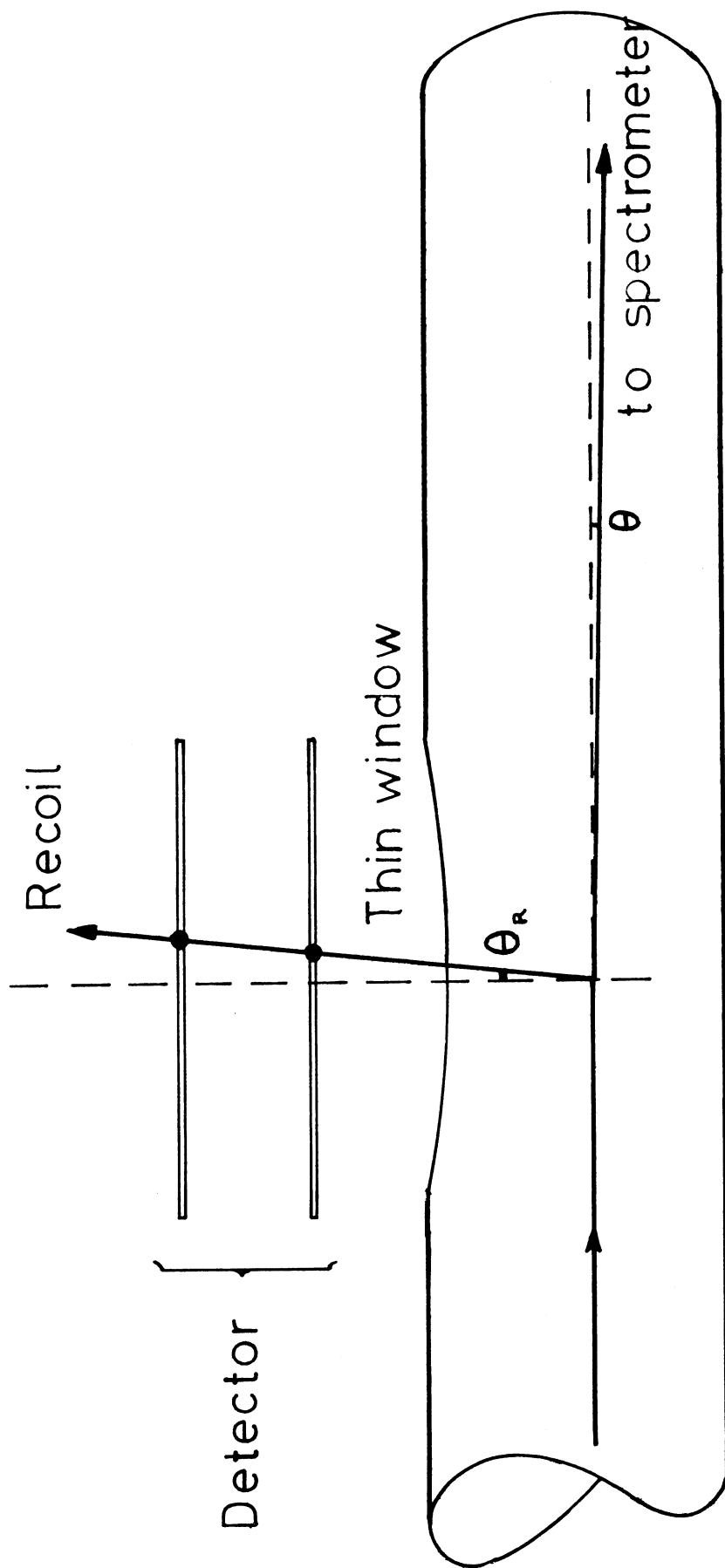


Fig. 19

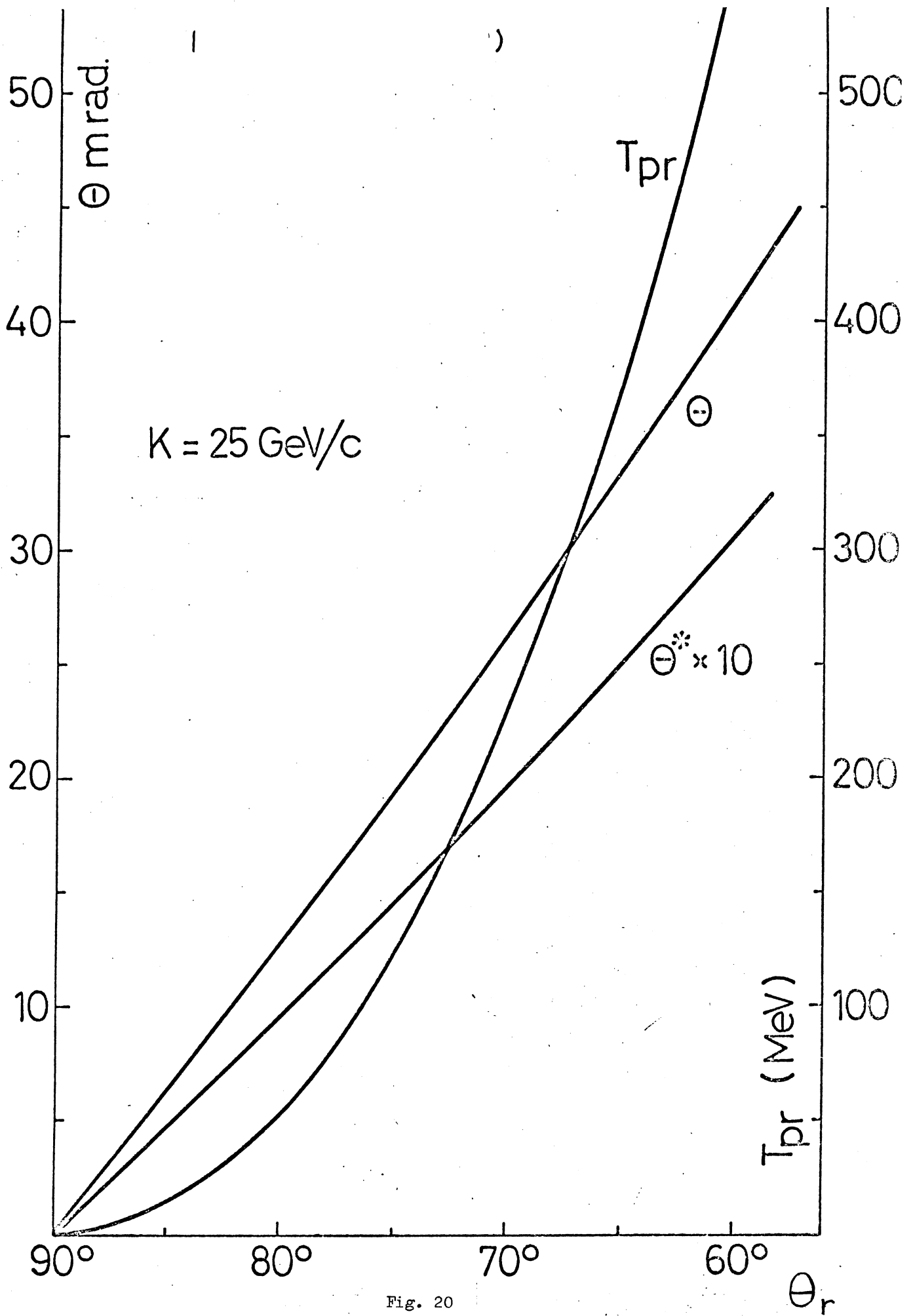


Fig. 20